Dynamical Climatology

The effect of improved physical parametrizations on simulations of cloudiness and the earth's radiation budget.

by

A. Slingo, R.C. Wilderspin and R.N.B. Smith

DCTN 65

April 1988

Meteorological Office (Met. O. 20)
London Road
Bracknell
Berkshire RG12 2SZ

DYNAMICAL CLIMATOLOGY TECHNICAL NOTE NO. 65

THE EFFECT OF IMPROVED PHYSICAL PARAMETRIZATIONS ON SIMULATIONS OF CLOUDINESS AND THE EARTH'S RADIATION BUDGET

by

A Slingo*, R C Wilderspin and R N B Smith

* Present affiliation: National Center for Atmospheric Research, Boulder, Colorado 80307, U.S.A.

Submitted for publication

Met O 20 (Dynamical Climatology Branch)
Meteorological Office
London Road
Bracknell
Berkshire RG12 2SZ U.K.

April 1988

NOTE: This paper has not been published. Permission to quote from it should be obtained from the Assistant Director of the above Meteorological Office branch.

ABSTRACT

The development of a new version of the United Kingdom Meteorological Office 11-Layer Atmospheric General Circulation Model is described, with particular emphasis on the prediction of the fractional cloud cover and of the earth's radiation budget. Results are shown first from an integration of an earlier version with model-predicted cloudiness. These demonstrate that there were serious shortcomings, particularly in the distribution of low cloud over the sub-tropical oceans. Analysis of this problem showed that it was due to systematic errors in the thermodynamic structure of the marine boundary layer. Various changes to the model's physical parametrizations were made to remove these errors, including revisions to the convection scheme to treat more accurately the effects of shallow cumulus convection. The new version of the model produces simulations of the geographical distribution of the components of the earth's radiation budget which are generally in good agreement with satellite measurements.

1. INTRODUCTION

It is common knowledge that clouds strongly influence the distribution of both the shortwave and longwave radiative fluxes, not only at the top of the atmosphere but also at the surface. The radiative forcing of the earth's climate system is thus in part determined by the distribution of cloudiness, which therefore must be taken into account in numerical models. Because of the temporal variability of cloud cover and the possible importance of cloud-radiation interactions in determining both the present climate and its response to perturbations, it is generally accepted that cloud fields need to be predicted within an Atmospheric General Circulation Model (AGCM) as an integration proceeds. Unfortunately, there is at present no reliable theory which can be applied to relate the cloud cover to the large scale variables used in such a model. Cloud prediction schemes thus depend mainly on empirical relationships (ECMWF, 1985; J.M. Slingo, 1987)

A parametrization scheme for fractional cloud cover was developed by J. M. Slingo (1980) for a limited-area tropical version of the Meteorological Office 11-Layer Model, based on experience with GATE data. This scheme performed satisfactorily in forecast integrations of three days duration. In longer integrations with the global model, a number of systematic errors in the mean cloud fields became apparent (Slingo, 1984). These errors will be discussed in the next section. In the present paper, the changes to the model which were found necessary to correct these and other deficiencies are described and simulations with a new version are presented. The model is being used for research into long-range weather forecasting and for climate simulation and sensitivity experiments lasting several years, using prescribed sea surface temperatures and sea-ice distributions. It is also being coupled to both an ocean general circulation model and to a sea-ice model for experiments on decadal time scales (Foreman, 1986).

The primary motivation for the work described here was the need to improve the simulated distributions of both cloudiness and radiative heating in the tropics (±30° latitude), although for completeness results

for the whole globe are shown. There are two main reasons why accurate simulations of cloud and radiation fields are particularly important at low latitudes;

Firstly, roughly two-thirds of the absorption of the incoming shortwave radiation which provides the energy source for the atmospheric and oceanic general circulations takes place within the tropics (e.g. Paltridge and Platt, 1976). Apart from clouds, the atmosphere is relatively transparent to solar radiation, so that over 70% of the absorption occurs at the surface, which in the tropics is primarily ocean. By reflecting solar radiation back to space, clouds thus strongly influence the heating of the ocean surface and thereby the sea surface temperatures (SSTs). Studies of the effect of SST anomalies have shown that they exert a profound influence not only on the tropical atmosphere but also on the circulation at higher latitudes (e.g. Palmer and Mansfield, 1986). It follows that in a coupled ocean-atmosphere model it is essential to predict realistic cloud distributions, as otherwise the SSTs would be adversely affected, with a consequent degradation of both the atmospheric and oceanic simulations.

Secondly, the effect of clouds on the Outgoing Longwave Radiation (OLR) is also greatest in the tropics. A typical value for the clear-sky tropical OLR is about 290-300 W m^{-2}. In regions of persistent deep cumulus convection, however, such as over Indonesia and South America from December to February ,the time-mean OLR is less than 200 W m^{-2} (e.g. Hartmann et al., 1986). Clouds are therefore responsible for a net longwave heating of the earth-atmosphere system, by on average about 100 W m^{-2} in these regions. In the longwave spectral region the tropical atmosphere is relatively opaque near the surface, owing to water vapour absorption, so that most of this cloud longwave forcing is felt within the atmosphere. The implied vertically-averaged contribution to the atmospheric diabatic heating is about 1 K/day, which is comparable to the contribution from latent heat release. Studies with a different AGCM confirm that the cloud longwave forcing can exert a strong influence on model simulations (Slingo and Slingo, 1988). It should be noted that this forcing is primarily atmospheric and so will be present even in a model with prescribed SSTs.

From the above it should be clear that the modelled distributions of the two components of the Earth's Radiation Budget (ERB) at the top of the atmosphere , namely the shortwave planetary albedo and the outgoing longwave radiation, should be as realistic as possible. These fields may be compared with measurements made by satellites (Hartmann et al., 1986). Data from the Nimbus 7 ERB experiment are used here (Kyle et al., 1985), these being the most reliable data generally available at the time this work was carried out. The emphasis in the work reported here was on using the ERB fields from the model as diagnostic tools for identifying areas where the model's physical parametrizations were inadequate. Two important improvements which were made were firstly to modify the convection scheme so that it could represent the effects of shallow cumulus convection more accurately and secondly to include a revised formulation of sub-gridscale turbulent exchanges which explictly predicts the number of model layers within the atmospheric boundary layer. It is shown that these and other changes substantially improve the model's cloud and radiation budget climatology at low latitudes, and at the same time allow the cloud prediction scheme to be simplified compared with the original version. The latter is believed to be an important result, as several studies being carried out with the model are concerned with analysing the role of cloud radiative forcing and feedbacks in the response of the model to a perturbation. With a simpler cloud scheme it should be easier to understand how those feedback processes are operating. This is particularly important in research on the impact of increasing carbon dioxide concentrations, where the role of cloud feedbacks has been identified as being one of the major areas of uncertainty (Wetherald and Manabe, 1986; Schlesinger and Mitchell, 1987).

2. INITIAL INTEGRATION WITH INTERACTIVE CLOUD

a) Model and cloud scheme

The version of the 11-Layer Model employed for the first extended integration with model-predicted cloudiness was the control described in Table 1 of Slingo and Pearson (1987). The only differences were that the time-smoothing coefficient α had the value 0.005 rather than 0.01 and the cloud cover was predicted rather than prescribed. Basic details of the model are given in Slingo and Pearson (1987), which also refers to earlier detailed descriptions of individual parametrizations.

The cloud scheme was the same as that described by J. M. Slingo (1980), apart from the changes noted in the next paragraph. This scheme predicts the fractional amount of layer (or large-scale saturation) clouds, which are one model layer in thickness, and of convective clouds, which may be any number of model layers deep. The capability of modelling a convective cloud tower extending through several model layers is an important feature of the scheme, although it leads to additional complexity in the radiation calculations. The tower is designed to represent the deep clouds associated with vigorous penetrating convection, which are of course especially important in the tropical regions. The common assumption is made of random overlap between clouds in different model layers, but if both convective and layer clouds are present in the same model layer then their radiative effects are essentially additive. If the convective tower extends through two or more layer clouds, then the latter overlap only in the clear air remaining around the tower. The convective cloud amount was obtained from a linear dependence on the maximum saturated mass flux calculated in the model's convection scheme, with different relationships for land and sea points (J. M. Slingo,1980; Equations 1 and 2). If the cloud depth exceeded three layers then the amount was reduced by a factor of ten and the remaining 90 per cent added to the low cloud field. This was intended to represent the fact that cumulonimbus clouds occupy a small fraction of the area covered by a tropical disturbance, but are associated with substantial amounts of shallower clouds at low levels.

In the original cloud scheme described by J. M. Slingo (1980), layer cloud amounts are predicted from a quadratic dependence on the relative humidity. In addition, the persistent sheets of stratocumulus over the sub-tropical oceans were represented by a dependence of the low cloud amount on the potential temperature lapse rate. For the initial integration reported here, the latter dependence was removed. In earlier short test experiments it had been found that this term contributed to a considerable over-estimate of the cloud amount in these areas. It will be seen later that this was due to unrealistically strong inversions, but it was also found to be extremely difficult to tune the low cloud amounts, given the double dependence on both relative humidity and lapse rate. The relative humidity used to calculate the amounts of low, medium and high layer cloud was also changed from the grid-box average value to an adjusted value representative of the clear air between any convective clouds at that level (i.e. of the environmental air). Cloud amounts increased quadratically from zero at the threshold relative humidity to full cover at saturation. From previous experience with the global model, the threshold relative humidity was set to 85 per cent for all layer clouds to give a globally-averaged cloud cover of about 50 per cent. Low cloud was defined to be in layers 10 and 9, medium cloud in layers 8 to 6 (only 8 and 7 poleward of 60° latitude) and high cloud in layers 5 to 3 (6 to 4 poleward of 60°), as illustrated by Fig. 4 of J. M. Slingo (1980). In this integration, clouds were not allowed in the top two layers or the bottom layer.

The division of the layer cloud field into three categories was made originally to facilitate comparison with conventional surface-based observations (J. M. Slingo, 1980). The radiation scheme was therefore designed to deal with no more than three layer clouds at any instant, i.e. one in each of the categories High, Medium and Low. For each category, the cloud is therefore assigned to the layer with the highest relative humidity, and hence the highest predicted cloud amount. For example, if 86 per cent cloud cover is predicted in layer 9 and 60 per cent in layer 10, then the low cloud amount is taken to be 86 per cent in layer 9. There is of course a danger that clouds may form and persist preferentially in certain layers. Some evidence of such problems is presented later.

The radiative properties of the clouds in the 11-layer model were originally the same as the values used in integrations of the 5-Layer Model (J. M. Slingo, 1982) but were modified following comparisons with satellite ERB data (Slingo, 1985a). The values assumed for the initial integration are listed in Table 1.The values are not unreasonable given the observational data summarised by Feigelson (1984). The relationship between the albedo and emissivity of high cloud is also consistent with the work of Stephens and Webster (1981). No dependence on solar zenith angle or cloud liquid water path was included, although both have been implemented in versions of the NCAR Community Climate Model (Ramanathan et al., 1983; Charlock and Ramanathan, 1985). It is accepted that these and many other factors, such as the cloud shape and drop size distribution, are responsible for wide variations in cloud radiative properties (Welch et al., 1980; Crane and Barry, 1984; Herman and Curry, 1984). However, there are still significant differences between observed and modelled values, especially for cloud shortwave absorption (e.g. Stephens et al., 1978), except in the unusual case of a uniform sheet of non-precipitating stratocumulus (Slingo et al., 1982). In addition, with the exception of the cloud liquid water path, none of these cloud properties can be predicted with confidence in current AGCMs. In the face of such uncertainties it was decided to use fixed radiative properties for the present study, leaving only the cloud amount to be predicted. In an important extension of this work, however, the model has been further modified to carry an explicit cloud water variable (Smith, in preparation). In the future, it should therefore be possible to predict the cloud radiative properties from the cloud water amounts, provided that the latter values are reasonable.

The surface shortwave albedos which were assumed are similar to those used in the 5-Layer Model (J. M. Slingo, 1982) and are listed in Table 2. The temperature dependence of the sea-ice albedo crudely represents the tendency for leads to open through the ice and for meltwater ponds to form on the surface as the grid-box mean temperature increases. Similarly, the dependence of the albedo of snow-covered land on the snow depth is designed to take account of the fact that as the mean snow depth increases, not only

does the snow more completely cover any surface irregularities but also the area of the grid box which is snow-free is likely to decrease. The geographical distribution of the snow-free land albedo was derived by Wilson (1984) from the global dataset of land cover and soils data compiled by Wilson and Henderson-Sellers (1985).

The model was integrated with seasonally-varying forcing at a horizontal resolution of 2.5° x 3.75° (latitude x longitude) with prescribed sea surface temperatures and sea-ice distributions, as in the experiments described by Slingo and Pearson (1987), in this case through two annual cycles. Selected results are shown in Figs. 1-5. These are primarily from the northern summer season in order to keep the number of figures to a minimum.

Throughout this paper, both the model and observational data are shown at a resolution of 5° x 5°. This is partly to enable the comparison of the ERB data with those from Nimbus 7 (see below). There is the additional benefit that the maps are more readable at the size reproduced here than the original model data would have been. The model's land-sea mask and latitude and longitude lines every 30 degrees are also shown.

b) Results

The radiation budget is compared with data from the Nimbus 7 ERB experiment (Kyle et al., 1985). Data from the Wide Field Of View (WFOV) instrument have been gathered continuously since 1978, but at low horizontal resolution. The Narrow Field Of View (NFOV) data are preferred here, as these were obtained with the higher resolution scanner instrument. Unfortunately, this operated for only 20 months and so the results do not give a reliable long-term radiation budget climatology. A useful comparison between WFOV and NFOV data which demonstrates the smoothing effect of the former is shown by Ramanathan (1987, Fig. 11). Both the WFOV and NFOV data are broad-band measurements and so do not suffer from the well known uncertainties which are inherent in the derivation of broad-band fluxes from the narrow band NOAA AVHRR data (e.g. Hartmann et al., 1986, section 3). The NFOV data were obtained from the MATRIX tapes, where the

horizontal resolution is about 500 km, and were corrected for calibration errors (Kyle et al., 1985). The OLR values were increased everywhere by 3.1 Wm^{-2} and the shortwave albedos were divided by a factor of 1.09. The Nimbus 7 data shown in Figs. 1 and 3 (and later in Figs. 13 and 14) are the same as those presented in a different projection by Hartmann et al. (1986, their Figs. 4 and 5), except that they did not correct the data.

Of interest in the observed OLR distribution in the northern summer season (Fig. 1(a)) is the strong symmetry about the ITCZ at 10-15°N and the sharp latitudinal gradients in the western hemisphere. This pattern, with a well-defined ITCZ and symmetric areas of enhanced emission associated with the sub-tropical highs in both hemispheres over the Atlantic and Pacific oceans, may also be seen in the 10 year OLR dataset derived from NOAA satellite data (Janowiak et al., 1985). The pattern is radically different in the eastern hemisphere because of the Asian summer monsoon. The modelled distribution (Fig. 1(b)) is in reasonable agreement with the observed. The minima at low latitudes coincide with regions of deep convection. Detrainment from the convection scheme in the upper troposphere leads to high relative humidities and hence the prediction of significant amounts of high cloud, representing the extensive cirrus seen on satellite images. The distributions of OLR (Fig. 1(b)) and precipitation (Fig. 2(b)) are thus highly correlated at low latitudes, although this is less evident over the west Pacific, because of smaller amounts of high cloud compared with, for example, over the Indian ocean. The precipitation distribution is also in reasonable agreement with Jaeger's (1983) climatology (Fig. 2(a)). The model reproduces the enhanced longwave emission in the sub-tropical dry zones, although the maxima over the oceans are up to about 20 W m^{-2} larger than in the satellite data. For example, there are areas over both the Atlantic and Pacific oceans where the modelled emission exceeds 300 W m^{-2} (Fig. 1(b)). The decrease in OLR towards the poles is also realistic, although the modelled values are too low over the North Pole.

In contrast, the modelled distribution of the shortwave planetary albedo is poor at low latitudes (Fig. 3(b)). There are maxima over the sub-tropical oceans in both hemispheres where in the observations there are

minima (Fig. 3(a)). To the east of these regions, notably adjacent to South America and southern Africa, there are minima where in reality the persistent sheets of stratus and stratocumulus produce albedo maxima. These errors are caused by deficiencies in the low and convective cloud distributions (Fig. 4). Spurious cloud maxima occur where in addition the precipitation rates are in excess of observed values (Fig. 2). Similar errors in the precipitation fields were noted in the integration with prescribed cloudiness described by Slingo and Pearson (1987, their Fig. 7). The fact that this over-estimate occurs with both fixed and interactive cloudiness indicates that the cloud maxima are not caused by deficiencies in the cloud prediction scheme but by a more fundamental model error. In the next section, evidence is presented that this error is due to an inability to represent the effects of shallow cumulus convection, and changes to include such a process are described.

A second problem evident in Fig. 3(b) is that the albedo maxima over the main tropical precipitation areas are missing or very weak. This is mainly due to a lack of convective and low cloud (Fig. 4), for reasons which are discussed further in section 3(b).

The errors in the cloud fields described above are serious in their effect on the albedo distribution, but they make only a minor impact on other aspects of the model's simulation. Indeed, as far as the dynamical fields and precipitation distributions are concerned, the results are little different from the control integration with prescribed zonally-averaged cloudiness described by Slingo and Pearson (1987). The reason is that with fixed SSTs the errors in the surface shortwave radiative forcing over the oceans are ignored by the model, which responds only to the much smaller changes in the atmospheric heating rates. In a coupled ocean-atmosphere model, however, the SSTs change in response to the surface forcing, so it is necessary for the latter to be as accurate as possible. This provided the primary motivation for improving the low and convective cloud fields.

The importance of a realistic distribution of low cloud over the sub-tropical oceans from a model which is to be coupled to an ocean GCM is illustrated in Fig. 5. This compares the estimates by Esbensen and Kushnir (1981) of the annual-mean heating of the ocean surface (Fig. 5(a)) with the data from one year of the annual-cycle integration (Fig. 5(b)). Other climatological datasets have been published by Weare et al. (1981) and Hsiung (1985). The estimates all have large error bounds (in places as big as 100%), which reflect the difficulties inherent in such studies, although the patterns in the different climatologies are broadly similar. The observed data demonstrate that in the annual mean the tropical oceans receive an excess of energy, due to the incoming shortwave radiation being a maximum there. This excess is transported by the oceanic general circulation to higher latitudes, where it is released to the atmosphere in the shaded areas of net surface cooling. The areas with the largest negative values occur over the western boundary currents in northern mid-latitudes, where the primary heat loss is by the upward turbulent heat and moisture fluxes. There are also minima in the sub-tropics due to semi-permanent cloud features such as the sub-tropical stratocumulus in the eastern north Pacific and southeast Atlantic oceans and the cloud in the South Pacific Convergence Zone. The clouds in these areas reflect the incoming shortwave radiation back to space, reducing the surface heating. This effect is larger than the opposing longwave warming, caused by the increase in the downward longwave flux at the surface compared with clear skies.

In the model, the distribution is seriously distorted by errors in the cloud fields. The effects of the maxima in the low and convective cloud fields (Fig. 4) are clearly visible. The pattern of surface heating is altered so radically that if this version of the model were to be coupled to an ocean GCM one would expect large errors in the sea surface temperature field, with consequent errors in both the oceanic and atmospheric general circulations. Efforts to improve the cloud distributions were thus given a high priority and the changes made to the model will now be described.

3. CHANGES TO THE MODEL

In the previous section, three serious errors were identified in the cloud distributions: excessive amounts of cloud at low levels over the central sub-tropical oceans, a failure to represent the convective cloud associated with deep tropical convection and a deficiency of low cloud in the sub-tropical marine stratocumulus regimes. The first four of the changes to the model described below were designed to alleviate these problems. Some of the changes described afterwards were also aimed at improving the cloud and ERB fields, but other improvements not directly related to those fields were also included, such as the parametrization of orographic gravity-wave drag and the new land surface model. Table 3 summarises all the changes and the reasons for their inclusion, the order being the same as in the following sub-sections. A large number of integrations up to two years in length were made to test the changes as they were introduced one by one. This facilitated the isolation of the effects of individual improvements as well as any necessary adjustments.

a) Shallow convection: "Split final detrainment"

Examination of the model's thermodynamic structure in the areas of excessive low cloud showed that the cloudy layer immediately below the top of the boundary layer was close to saturation and was surmounted by a strong and extremely dry inversion. The equivalent potential temperature (θ_e) decreased by up to 16K through the inversion (see also Fig. 7 of Slingo and Wilderspin (1985) and the associated discussion). This indicated that there was insufficient mixing between the boundary layer and the free atmosphere, as such a large θ_e lapse rate is unstable to moist mixing processes. The low layer cloud satisfied the criterion for the onset of Layer Cloud Instability (LCI), which Randall et al. (1985) employed to prevent such unrealistic behaviour in the UCLA model. A parametrization of LCI was developed for the 11-Layer Model, but after some test integrations it was removed as not only was the physical basis difficult to justify but also it was found to be operating in areas where mixing would be expected to be through convective rather than LCI processes, for example in the trade-wind cumulus regimes.

In the trade-wind areas, cumulus clouds transport boundary layer air into the free atmosphere and vice versa and thus prevent large-scale saturation from occurring (Augstein, 1979), as was clearly demonstrated in BOMEX (Barbados Oceanographic and Meteorological EXperiment; Holland and Rasmusson, 1973). BOMEX was carried out in the northern summer season (at the end of June 1969) at about 15°N 56°W. Figures 3 and 4 show that at this time of year the model produced excessive amounts of boundary layer cloud in this region. It is thus instructive to compare the model's mean thermodynamic structure with that observed during BOMEX. In the BOMEX data (Fig. 6(a)), the temperature profile follows the dry adiabatic lapse rate up to about 950 mb, whence scattered cumulus clouds were observed extending into the trade inversion. The region above the inversion was drier and as a result θ_e decreased by about 10 deg K compared with the value in the upper part of the boundary layer. In the model (Fig. 6(b)), the boundary layer is more nearly saturated at about 850 mb and the temperature inversion is stronger. The dew-point lapse is very much larger than in the BOMEX data, so that θ_e drops by 16K through the inversion. From this comparison it is clear that the cooling and moistening of the layer above the inversion (and the compensating warming and drying of the boundary layer) by the penetrating cumulus convection was not being represented by the model. This is in spite of the fact that moist convection was taking place within the model's boundary layer, as evidenced by the significant amounts of convective cloud shown on Fig. 4(b). The reason is that in the original version of the model's convection scheme, when convective parcels encountered a stable region, such as the trade-wind inversion, which they could not penetrate to rise to the next model layer, they detrained completely in the lower layer (Rowntree, 1984; Cunnington and Rowntree, 1986). Shallow convection within the boundary layer could thus lead to no interchange with the free atmosphere if an inversion was present, so the boundary layer remained too moist. Without the effects of cumulus detrainment above the inversion, there was also no process to offset the drying and warming effects of the large-scale subsidence. A modification to the scheme to model such interchange by allowing a fraction of the parcels to reach the next layer is described below. A similar problem was found in the ECMWF model (Tiedtke, 1984; Tiedtke et al., 1988). Rather

than change the convection scheme in the ECMWF model, Tiedtke formulated an additional parametrization of "shallow-convection". The effects on the thermodynamic structure of that model are similar to those discussed for the new version of the 11-Layer Model in section 4.

A brief description of the original version of the convection scheme is given by Cunnington and Rowntree (1986). A more complete account, including the equations, is contained in the model handbook (Slingo,1985b), in Bell and Dickinson (1987) and in a paper being prepared for the open literature (Gregory, personal communication). In this and the following sub-section, only so much detail is given as is necessary to explain the changes which were made.

The penetrative convection scheme used in the model is based on parcel theory modified by entrainment and detrainment. The parcel represents an ensemble of buoyant plumes, each with different characteristics. Parcel values of temperature, mixing ratio and mass flux are thus averages over the ensemble. The scheme is applicable to both dry and moist convection.

Working upward from the surface, each model layer is tested until one is found in which air with a slight excess of buoyancy (0.2K) is still buoyant at the next layer, after the entrainment of environmental air during ascent has been accounted for. If the buoyancy exceeds a lower limit (0.2K) then convection is initiated, the initial mass flux of the parcel being proportional to the excess buoyancy.

Ascent continues until the parcel being lifted from layer k is not buoyant in the next model layer (k-1). It is then assumed that a proportion of the plumes represented by the parcel have reached their zero buoyancy level and are detraining. The proportion of the plume detrained in layer k is assumed to be sufficient to allow the parcel to be just buoyant (by 0.2K) in the next layer above. This process allows the buoyancy to increase indefinitely and so is limited by two constraints . Firstly, a parcel cannot ascend higher than an undiluted parcel from the convective starting level. Secondly, if the mass flux falls below a minimum value then the parcel is assumed to be destroyed by detrainment.

In the original version of the scheme, when convection is terminated the detrainment takes place in layer k only . As illustrated in Fig. 7, this is a poor approximation in regions where shallow convection acts as a link between the boundary layer and the free atmosphere, as it fails to produce any modification of the inversion air. In reality, a fraction of the ensemble (i.e. the most buoyant plumes) penetrate the inversion and detrain boundary layer air above it. In the modified version of the scheme, part of the ensemble detrains in layer k with neutral buoyancy and the remainder in layer k - 1 with parcel values. The final detrainment of the ensemble is thus split between layers k and k - 1, which explains the name for this modification. It will be shown in section 4 that this modest, but physically reasonable, change leads to a substantial improvement in the thermodynamic structure and low cloud fields over the sub-tropical oceans.

b) Calculation of convective cloud cover

As noted in Section 2, the areas of convective cloud associated with deep convection and high precipitation in the tropics are missing from Fig. 4(b). This is in part because, for reasons concerned with minimising the computer core space occupied by model variables, the convective cloud cover was diagnosed from a separate call to a version of the convection scheme from within the radiation scheme. Since this preceded the point at which the surface fluxes were applied to the lowest model layer, the magnitude of the diagnosed convective activity was in most areas much less than that actually occurring in the model. For the new integration, an enhancement to the main memory of the Cyber 205 allowed the convective cloud amount to be calculated from the call to the convection scheme actually used by the model. In addition, the method for calculating the cloud amount was revised completely. In the original scheme, the convective cloud amount was calculated from a linear dependence on the maximum saturated mass flux in the convective parcel (J.M. Slingo, 1980). Following the changes to the convection scheme described in sub-section (h) below, it was decided to revise the method and in particular to make use of the calculation of the total liquid water content of the parcel. After some experimentation, it

was found that a logarithmic relationship gave both reasonable looking global cloud fields and also a close correspondence at low latitudes between the convective precipitation and cloud amounts;

$$C_C = 0.5 + 0.06 \ln W \qquad \text{for } W \geq 2.404.10^{-4} \qquad (5)$$
$$= 0 \qquad \text{otherwise}$$

where C_C is the fractional convective cloud amount and W is the total parcel liquid water path, prior to precipitation, in Kg m^{-2}. Unlike the original scheme, no distinction is made between shallow and deep convection, so that the reduction in the cloud amount for deep clouds and the enhancement of the low cloud field were removed. As with other changes to the cloud scheme, this was done to reduce the complexity in order to test the viability of a very simple scheme.

c) New boundary-layer scheme

As noted earlier, in the initial integration there was very little cloud predicted in the areas of persistent sub-tropical marine stratocumulus. This was mainly due to the boundary layer scheme used, which is described by Carson (1982a,b). Within the Ekman layer it is based on the recommendations of Clarke (1970) and is therefore referred to as the "Clarke" scheme. The vertical turbulent fluxes of heat, moisture and momentum are computed by an eddy diffusivity approach. The mixing lengths depend on the stability of the surface layer and turbulent mixing takes place throughout the lowest three layers of the model, the boundaries of which are noted in Table 4. Such a scheme does not take account of variations in boundary layer depth and as a result the boundary layer in the stratocumulus regimes was too deep and too dry, leading to the prediction of negligible amounts of low cloud.

For the new version of the model, this scheme was replaced by one developed by Richards (1980). A brief description is given by Mitchell and Slingo (1988) and full details are given in the model handbook (Slingo, 1985b). The "Richards" scheme uses different functional forms for the mixing lengths and these depend on the local Richardson number where the

turbulent fluxes are calculated. The presence of a stable layer can thus be detected, such as an inversion at the top of the boundary layer, and mixing restricted to the underlying atmosphere. In effect, the scheme diagnoses the depth of the planetary boundary layer, in terms of the number of model layers experiencing turbulent mixing. In regions where subsidence and/or radiative cooling create a near-surface inversion, such as at night over land and over the relatively cold water near the eastern boundaries of the sub-tropical oceans, the boundary layer may thus be only one layer deep. By using this scheme and in addition allowing low cloud to form in the lowest model layer (see next sub-section) the stratocumulus was predicted, as demonstrated in section 4a. The boundary layer depth is itself an important diagnostic of this scheme and will be discussed later.

d) Revised treatment of layer cloud

In the initial simulation, clouds were not allowed in either the lowest layer or the top two layers. Such restrictions could create problems in climatic change experiments, as they might distort the response of the model to a perturbation. In such experiments the cloud scheme should ideally include no such artificial constraints. Cloud is now allowed in every layer of the model, except the top layer, which should not pose problems for reasonable perturbations. By allowing cloud to form in the lowest layer, the areas of sub-tropical stratus/stratocumulus can also be represented better.

e) Surface albedos increased over the Sahara

Over the Sahara, the modelled planetary albedos shown in Fig. 3(b) are lower than the observed values. In this region cloud amounts are small, but the relatively high surface albedo of the desert leads to observed planetary albedos exceeding 30 per cent. This suggests that the model's surface albedos were too low. Examination of the surface albedo field used in the model showed that there were values of 31 or 35 per cent over most of the Sahara, but values of 21 per cent in some areas. The latter value is much lower than, for example, those derived by Geleyn and Preuss (1983) from satellite data, which exceed 30 per cent throughout the Sahara. It

was also noted that the additional surface heating brought about by these low albedos relative to surrounding grid-points led to enhanced convergence of moisture into the region from the south and hence to areas of anomalously high precipitation. One of these is visible in Fig. 2(b) just east of the Greenwich meridian. A similar sensitivity of the Saharan climate to the surface albedo was also noted by Cunnington and Rowntree (1986). It was therefore decided to increase the surface albedo for these points to 31 per cent in the new version of the model.

f) Emissivity of high cloud reduced

Examination of results from preliminary versions of the new model showed that, over regions of tropical deep convection, the outgoing longwave radiation tended to be lower than the observed while the shortwave albedo was reasonable. The distribution of high cloud was satisfactory (as will be seen for the new model in the next section), so the emissivity of high clouds was reduced from 0.75 to 0.6. All the other cloud radiative properties listed in Table 1 were unchanged. Despite this reduction, the relationship between the high cloud albedo and emissivity is still consistent with Stephens and Webster (1981).

g) Revised albedos for sea-ice

Experience with a version of the atmospheric model coupled to a slab ocean, for investigations of the effect of doubled CO_2 concentrations on climate (Wilson and Mitchell, 1987), showed that the simulation of sea-ice extents was sensitive to the assumed sea-ice albedo (Mitchell, personal communication). Various revisions of the formulation noted in Table 2 were tried. In the final version, the albedos were reduced by changing the limiting values 0.8 and 0.5 (at 268K and 273K) to 0.7 and 0.4, respectively.

h) Convection scheme : other changes

A further group of changes to the convection scheme were included in the new model. The first part consists of a further detrainment term to model the effects of mixing processes near the edges of updraughts, which transfer air both into and out of the buoyant plume. The second part involves changes to the treatment of the evaporation of cloud water and precipitation. These changes were made in response to the strong sensitivity found in earlier integrations to the formulation of the evaporation (Rowntree, 1984) and to experience with the scheme in the operational numerical weather prediction model, described by Gadd (1985). In the latter model, there was too much precipitation from shallow convective clouds over the northern continents in summer. To overcome this, cloud water is now retained within the clouds (i.e. precipitation is inhibited) until the cloud reaches a critical depth, taken to be 4 km over land, 1.5 km over the sea and 1 km when the environmental temperature is less than 263 K. Further details are given by Slingo (1985b) and Bell and Dickinson (1987).

In the original version of the scheme, the evaporation of convective precipitation into an unsaturated environment was allowed both below cloud base and within the cloud, the latter being intended as a simple representation of downdraughts. For the new model, the evaporation was restricted to below the cloud base. Consideration is being given to a more comprehensive formulation of the effects of convective downdraughts (Gregory, personal communication).

i) New land surface model

In common with most AGCMs, the 11-Layer Model has employed a very simple land surface model (Carson, 1982b). With increased awareness of the importance of land surface processes in climate, much effort has been put into improving the model in the areas of surface temperature prediction and hydrology.

The land surface temperature in the initial integration was modelled by considering the energy budget of a single slab. The net surface heat flux was converted into a temperature change per timestep by assuming that the slab had a thermal capacity equivalent to that of 5 cm of water, which is designed to give a reasonable amplitude to the diurnal cycle of the surface temperature. This was replaced by a 4-layer model, in which the thickness and properties of each layer are chosen so as to optimise both the amplitude and phase response to forcing over a wide temporal range from below the diurnal to beyond the annual cycles (Warrilow et al., 1986; Mitchell and Slingo, 1988).

As with surface temperature, the treatment of hydrological processes has also been very simple. Following Manabe (1969), the water balance of a single soil moisture store is considered. The soil moisture content is increased by precipitation and snowmelt and decreased by evaporation. In the original version of the model, once the soil moisture content reaches 15 cm any further increase is ignored and is deemed to contribute to runoff. This simple scheme allows the model to represent the strong influence of the availability of soil moisture on evaporation, and hence on the surface energy budget. However, it is obviously very crude and as a first step was replaced by a new hydrological model (Warrilow, 1986). This includes a term for rapid surface runoff, when the rainfall rate exceeds the infiltration rate, and one for the slow gravitational drainage of existing soil moisture. The upper limit on the soil moisture content was removed, so that values above 15 cm can occur.

j) Evaporation of large-scale precipitation

A simple parametrization of the evaporation of large-scale precipitation (formed when the grid-box humidity exceeds the saturation value) is included in the new model. This is partly for consistency with the convection scheme, which includes this process, although the formulation is different.

k) Orographic gravity-wave drag parametrization

Slingo and Pearson (1987) demonstrate that the parametrization of orographic gravity-wave drag developed by Palmer et al. (1986) leads to substantial improvements in the model's climatology in the northern hemisphere in winter.

l) New SSTs and sea-ice distributions

A new compilation of sea surface temperatures is used in integrations of the new model. These were interpolated to the model's grid from a preliminary version of a new climatology for 1951-80 (Folland et al.; in preparation).

m) Filtering of PMSL

The integration with gravity wave drag analysed by Slingo and Pearson (1987) suffered from a small-scale standing wave in the mass field, which grew during the integration. To avoid such problems, the PMSL (pressure at mean sea level) field is now smoothed every ten days by a 17-point filter. This has negligible meteorological impact, but prevents the build up of such unrealistic roughnesses. At the same time, the surface pressures are adjusted so as to force conservation of the globally-averaged mass.

n) Specification of the new version of the model

Table 4 gives a brief specification of the new version of the model. The cloud prediction scheme may be summarised as follows:

The layer cloud amounts C_L are predicted solely from the environmental relative humidity RH (i.e. that of the air outside convective clouds, which are assumed to be saturated).

$$C_L = \left(\frac{RH - RH_{crit}}{100 - RH_{crit}}\right)^2 \qquad \text{for } RH \geq RH_{crit} \qquad (6)$$

$$= 0 \qquad \text{otherwise}$$

The critical relative humidity is 90% in each model layer, except in the lowest layer where it is 95%. These thresholds are larger than in the initial integration (which used 85%, as noted in Section 2(a)) and were found to be necessary in order to tune the global-average cloud amounts and radiation budget.

The convective cloud amounts are predicted from equation (5) and the tops and bases are taken from the model layers in which the saturated convection begins and ends.

4. RESULTS FROM THE NEW VERSION OF THE MODEL

The results discussed in this section come from an annual-cycle integration of the new version of the model ("ACR4"). Data from 4 years of the integration were used to create seasonal and annual mean diagnostics. The simulations of the diurnal cycle of outgoing longwave radiation shown by Slingo et al. (1987) were from a development version of the new model, the main difference being that the new land surface parametrization (Section 3(i)) had not been implemented.

a) Cloud fields and related variables

The mean precipitation distribution for northern summer (Fig. 2(c)) differs in one important respect from that from the control integration (Fig. 2(b)). The sub-tropical dry zones now extend much further to the west over the oceans, in better agreement with Jaeger's data (Fig. 2(a)). This drying of the trade wind boundary layer is associated with substantial improvements in the low cloud and shortwave albedo distributions, as will be discussed shortly. One feature of Fig. 2(c) which is not realistic is the tendency for a precipitation minimum along the equator. This is especially noticeable over the west Pacific and Indonesia. This feature can also be seen to a lesser degree in earlier integrations, for example over the Indian ocean in Fig. 2(b). This is potentially an important problem, as the error is situated in a region where diabatic forcing exerts a strong influence on the general circulation.

In the low cloud field (Fig. 8(a)), the spurious maxima in the sub-tropics in the initial integration (Fig. 4(a)) have been removed. Over the BOMEX grid point, the tephigram from the new model (Fig. 6(c)) shows substantial changes to the thermodynamic structure, with a warmer and drier boundary layer and cooler and moister air above the inversion. The mean relative humidity at the top of the boundary layer is much lower than in Fig. 6(b), hence the removal of the excessive cloudiness.

The improvements noted above are consistent with those expected from the split final detrainment change to the convection scheme (Section 3(a)). In order to isolate the effect of this change, it was removed from an additional integration (RSFD) of the new model. Selected results for the northern summer season are shown in Fig. 9. Comparison of the total precipitation field with those in Fig. 2 shows that the change is indeed responsible for a substantial drying in the sub-tropics.

The low cloud field (Fig. 9(b)) shows that most of the spurious cloud in the sub-tropics in the initial integration (Fig. 4(a)) has re-appeared, with the global-mean low cloud amount increasing from 23.6% in ACR4 to 33.6% in RSFD. The substantial changes compared with Fig. 8(a) demonstrate the strong sensitivity of the low cloud field to the split final detrainment change.

However, the simulation in RSFD is intermediate between the initial integration and ACR4, indicating that some of the other changes are also contributing to the new model. A similar conclusion may be drawn from the ascent shown in Fig. 6(d), which is significantly different from the new model (Fig. 6(c)), but not as extreme as in the initial integration (Fig. 6(b)). One problem with these comparisons is that this grid point is close to the ITCZ, particularly so in the new model (see Fig. 2(c)), so that deep convective events are probably also contributing to the mean structure, whereas such conditions were omitted from the BOMEX study.

The areas of semi-permanent stratocumulus which extend westward from the coasts of north and south America and Africa are also represented in Fig. 8(a). The cloud is predicted in the lowest model layer, the boundary layer being only one sigma layer deep in these regions (Fig. 8(b)), in response to the subsidence associated with the surface high pressure cells and the weak surface heating from the relatively cold sea surface. At the grid points closest to the west coasts of south America and southern Africa, the boundary layer depths are thus below 500 m.

The boundary layer is also shallow over the polar regions, because of the low surface temperatures. As in the sub-tropics, there are significant amounts of low cloud in the lowest layer (Fig. 8(a)). Over the Arctic this agrees with the observations which show the greatest amounts of low stratus in this season (e.g. Warren et al., 1986). However, in the model the cloud persists throughout the year whereas in reality amounts in the winter season are much smaller. The low cloud also extends southwards over the northern hemisphere continents in winter. Low cloud is also excessive over Antarctica. Such problems indicate that the boundary layer is too moist in these regions. This could be due to the lack of a formulation of the entrainment of dry air into the top of the boundary layer, as well as the assumption that non-convective precipitation only occurs when the grid-box is completely saturated. The persistence of the cloud is probably also related to the strong cloud top longwave cooling, which is concentrated into a thin sigma layer.

The boundary layer depth map shows other interesting features in addition to those discussed above. Unlike all the other diagnostics shown in this paper, the depth was archived only from the values at the timestep corresponding to 00 hours GMT on each day. There is therefore some information on the simulation of the diurnal cycle, particularly over dry land areas. Over Africa, for example, the local time is around midnight, so the boundary layer is generally shallow in response to the surface nocturnal cooling. This is particularly noticeable over the Sahara desert, although over the tropical belt to the south the persistence of convection maintains a deeper boundary layer. Over the south-western United States the depth is much greater as the local time is late afternoon and convection is maintaining a relatively deep boundary layer. In the south Australian desert it is early morning and so the boundary layer is still shallow.

Over the oceans, the boundary layer is around 1 km in depth, being greatest where cold air from the continents is being advected over warmer sea. The latter phenomenon is particularly marked in the northern winter season (not shown) in the convectively unstable air over the western boundary currents of both the north Atlantic and Pacific oceans. The

boundary layer is shallowest in the stratocumulus regimes and deepens as a low level trajectory is followed from these areas around the sub-tropical highs into the ITCZ, in agreement with the observed behaviour (Riehl, 1979; Chapter 5).

The only other published simulations of the boundary layer depth with an AGCM are those shown by Randall et al. (1985, their Fig. 7). In general, their results are similar to those shown here, although the two boundary layer schemes are very different. In the 11-Layer Model, for example, entrainment at the top of the boundary layer is ignored, except that arising from convection. This is one area where further development of the model is being considered, in addition to the inclusion of a revised turbulent mixing scheme (Smith, in preparation).

The high cloud (Fig. 10(a)) and precipitation distributions (Fig. 2(c)) are strongly correlated, especially in the tropical regions where deep convection provides the moisture supply for these clouds. The effect of moisture transport at high levels away from the convection can also be seen. For example, in the ITCZ over both the Atlantic and Pacific oceans the high cloud is spread out further in latitude than is the precipitation. In addition, there is no minimum in the high cloud amount over the equator. There is generally more high cloud in this version of the model, particularly over Indonesia. The cloud amount is small in the sub-tropics but increases towards the poles, and in the mid-latitudes is largest in the storm tracks of both hemispheres. This seems reasonable as in reality significant amounts of frontal cirrus are observed in these regions (e.g. Warren et al. 1986). The medium cloud distribution (Fig. 10(b)) shows that the tropical convection is also moistening the middle layers of the model, although the amounts of cloud predicted are much smaller than at upper levels. In the high latitudes of each hemisphere there are enhanced amounts of medium cloud, although the patterns are fairly zonal in structure, even in the northern hemisphere.

The distribution of convective cloud amount (Fig. 11(a)) is much more reasonable than in the initial integration (Fig. 4(b)). There is now significant cloud cover in the areas of tropical deep convection and

smaller amounts in the trade wind regimes and at high latitudes. The amounts generally increase with the convective precipitation rate as expected from equation 5, although there is no exact correspondence between cloud amount and precipitation rate at the surface as the latter is affected by evaporation below cloud base. Although it is difficult to validate the exact form of the parametrization used, it does ensure a close link between the condensation rate and the radiative effects of the cloud and the distribution shown seems reasonable.

The distribution of convective cloud top pressure shown in Fig. 11(b) graphically illustrates the shallow and deep convective regimes. In the ITCZ and over much of the low latitude land areas, moist convection reaches on average to 400 mb or higher, the highest clouds achieving pressures of less than 200 mb over Central America and Indonesia. In contrast, over the sub-tropical oceans the shallow convection is generally well below 600 mb. Tnere is weak convective activity in the stratocumulus areas, but it is confined to below 800 mb. There are very strong gradients in the sub-tropics at the edges of the continents, where the climatic regimes change from suppressed conditions over the oceans to deep convection forced by strong surface heating over the land.

The zonal-average layer cloud amounts (Fig. 12) show the high cloud maximum forced by the deep convection at low latitudes. There is very little layer cloud below 400 mb in the tropics, which is probably unrealistic. The convective cloud contributes significantly in this area (Fig. 11), but that is mainly deep convection, so in general there is too little low cloud in the tropics. The sub-tropical stratocumulus shown in Fig. 8(a) occupies only a small area and so is not detectable on Fig. 12. At high latitudes in both hemispheres there are significant amounts of high, medium and low cloud, but the vertical distribution reveals a problem. There is a strong banded structure, with maxima at the lowest sigma layers in each category (0.317, 0.718 and 0.987 respectively). This structure is clearly spurious, although it is not known to what extent it degrades other aspects of the simulation. It is presumably the result of a general decrease in the mean relative humidity with height. Since the cloud prediction scheme places layer cloud in the layer with the highest

relative humidity in each category, this would tend to be the lowest layer, leading to the banded structure. This is an area where the design of the cloud scheme needs to be reconsidered.

b) Earth's Radiation Budget

The OLR and shortwave planetary albedo distributions for the northern summer season are shown in Figs. 1(c) and 3(c) respectively, where they can be compared with the results from the initial integration and from Nimbus 7. The OLR field is in better agreement with the Nimbus 7 data than that from the initial integration, with a more extensive shaded area representing values below 225 W m^{-2} over Indonesia. The regions over the sub-tropical oceans where the emission exceeded 300 W m^{-2} have also been removed. The basic pattern shown by the Nimbus 7 data is reproduced by the model, although the emission is too low from the high latitudes of both hemispheres. This might indicate that the atmospheric and surface temperatures are too low, but it could also be due to problems with the clouds (see below).

The improvements in the cloud fields lead to an albedo distribution which in the tropical belt is totally different from that in the initial integration and which now compares much more favourably with the observed (Fig. 3). The spurious maxima due to the excessive low cloud over the sub-tropical oceans have been replaced by minima, as observed. This improvement is mainly due to the split final detrainment change to the convection scheme, as can be seen by comparing the albedo map from experiment RSFD (Fig. 9(c)) with that from the new model in Fig. 3(c). The substantial increase in low cloud in RSFD noted earlier has produced a corresponding increase in the global-average planetary albedo, from 32.0% to 37.1%.

The new model also shows albedo maxima in the stratocumulus regimes, although these are somewhat weak and do not extend far enough to the west away from the coasts of South America and southern Africa. The ITCZ over the Pacific and Atlantic oceans and the maxima over the other areas of deep convection are also represented. Over Indonesia the albedo is higher than

in the initial integration, but is still somewhat lower than the observed. In both hemispheres, the albedos at high latitudes are larger than observed. Given that the OLR values are too low here, the problem may be due to excessive cloud amounts, although it is also probable that the assumed radiative properties are inappropriate for the low optical depth clouds to be expected in high latitudes. This would lead to errors in both components of the radiation budget, even if the cloud amounts were correct.

The two components of the radiation budget in the northern hemisphere winter are compared with Nimbus 7 data for 1979/1980 in Figs. 13 and 14. The modelled patterns are generally in very good agreement with the observed, although the errors noted above at high latitudes (albedo too large, OLR too low) may also be seen in this season. The albedo over the northern continents also shows a marked north-south gradient in Fig. 14(b) at about 40°N, which marks the edge both of the snow cover and of persistent and excessive low cloud amounts and, to a lesser extent, medium cloud amounts. In this season there is considerably less symmetry about the equatorial regions in both the observed and modelled radiation budgets in the western hemisphere. The South Pacific Convergence Zone (SPCZ) may be seen, extending south-eastwards from the ITCZ just west of the dateline over the southern Pacific ocean. A similar feature extends from the deep convection over South America over the south Atlantic. In the model these features are primarily due to enhanced amounts of medium and high cloud cover, as one would expect from the low OLR values.

The errors in the radiation budget at high latitudes exert a strong influence on the global means. The annual/global mean OLR at 224.2 Wm^{-2} is much lower than the Nimbus 7 value (235.8 Wm^{-2}) and the albedo at 33.0% is higher than the observed (30.2%). These errors tend to cancel in the net radiation (5.6 Wm^{-2} compared with 3.5 Wm^{-2}) which should be close to zero assuming no net heat storage. However, it would clearly be inappropriate to attempt to tune the two components of the global radiation budget to agree better with the satellite data before the high latitude problem has been reduced.

c) Annual-mean net surface heating

It was explained earlier in this paper that a primary motivation for the work reported here was to improve the distribution of the surface forcing, so that the model could be coupled to an ocean GCM and a sea-ice model to perform extended climate simulations. Although there are significant differences between the distribution of the annual-mean net heating of the ocean from the new version of the model (Fig. 5(c)) and that given by the Esbensen and Kushnir data (Fig. 5(a)), the heating is nevertheless considerably improved compared with that from the initial integration (Fig. 5(b)). In particular, the regions of spurious net surface cooling in the sub-tropics and tropics have either been removed or substantially reduced in intensity. Recent experience with the coupled model confirms that the improved physical parametrizations in the atmospheric model have had a beneficial impact on the ocean simulation. However, problems have arisen which may illustrate the sensitivity of the surface heating to the shortwave radiative component and hence to the cloud amounts and albedos. Firstly, in the global coupled model, sea surface temperatures (SSTs) tend to be too low and sea-ice too extensive at high latitudes (S. Foreman, personal communication). This is probably due to the excessive planetary albedos, so that too much of the incident shortwave radiation is reflected back to space, producing anomalous surface cooling. Secondly, tropical SSTs (in particular those in the west Pacific) tend to be too high, especially in a limited area tropical ocean model (C. Gordon, personal communication). This is to be expected from Fig. 5(c), which shows net heating exceeding 60 Wm^{-2} in the west Pacific, compared with only about 20 Wm^{-2} in Fig. 5(a). It is not clear whether this is due to excessive net radiative heating of the surface or to an underestimate of the cooling by surface evaporation. However, the cloud distribution may well be partly responsible, as the modelled planetary albedos tend to be somewhat lower here than the observed, especially in the northern summer season (compare Fig. 3(c) with 3(a) and 14(b) with 14(a)), so that too little (or too transparent) cloudiness may be allowing too much shortwave heating of the surface.

5. DISCUSSION

It has been demonstrated that the revised physical parametrizations have improved significantly the cloud and radiation budget simulations from the 11-Layer Model, although several deficiencies remain which need to be understood and rectified. It has also been possible to reduce the complexity of the cloud prediction scheme, which is regarded as desirable in a climate model because of the need to understand how changes in the cloudiness are induced by a perturbation and also given the somewhat arbitrary nature of diagnostic cloud schemes. However, the importance of cloud forcing and feedback in climate is such that it would clearly be unwise to rely solely on the version of the model developed here. In addition, the assumption of fixed cloud radiative properties is restrictive, particularly as changes in these properties are to be expected during climate change (e.g. Roeckner et al., 1987). More recent work has therefore concentrated on the development of a prognostic cloud prediction scheme, in which the cloud liquid water/ice content is held as an additional model variable. Results from this version of the model will be presented in a future paper (Smith, in preparation). In addition, a new scheme for predicting the radiative properties of water clouds is being developed and it is intended to couple this to the prognostic cloud scheme so that the properties are interactive with the rest of the model.

The sensitivity of the model to the treatment of shallow convection is in agreement with the results obtained with the ECMWF forecast model by Tiedtke et al. (1988). Given the apparent importance of shallow convection to the structure of the tropical boundary layer, it is surprising to find that both in their study and the present one, the observational data employed for comparison were obtained almost 20 years ago (ATEX and BOMEX were conducted in 1969). A further study of the mean thermodynamic structure and energy transfers in the trade-wind regions would appear to be long overdue. A related area where it is expected that new observations should aid the development of physical parametrizations is in the stratocumulus regimes. Fortunately, with the recent completion of the FIRE (First I.S.C.C.P. Regional Experiment) stratocumulus field experiment off the Californian coast, much useful data should soon be available (Cox et.

al.,1987). These data will be of particular value to climate modellers given the importance of these regions to the heat balance of the oceans. Only through the continuation of such field studies will it be possible to generate the database which is essential for the development and verification of physical parametrizations in numerical models.

ACKNOWLEDGEMENTS

The changes to the convection scheme described in Section 3 were devised by P. R. Rowntree. We are grateful to Dr. H. Lee Kyle of the NASA Goddard Space Flight Center for making available a tape of the Nimbus 7 Earth Radiation Budget (ERB) data, to S. Brentnall and C. Lakeland for assistance in producing the figures and to many of our colleagues for their comments on the manuscript. The integration omitting the split final detrainment in the convection scheme was run by E. Buckley.

REFERENCES

Augstein, E., 1979, The atmospheric boundary layer over the tropical oceans, Meteorology over the tropical oceans, pp 73-103, Royal Meteorological Society, Bracknell.

Bell, R.S. and A. Dickinson, 1987, The Meteorological Office operational numerical weather prediction system, Meteorological Office Scientific Paper No. 41, Her Majesty's Stationery Office, London.

Carson, D.J., 1982a, Comments on the sensitivity of numerical simulations to different parametrizations of the boundary layer properties and processes, Workshop on Planetary Boundary Layer Parametrization, pp 119-153, 25-27 November 1981, ECMWF.

Carson, D.J., 1982b, Current parametrizations of land surface processes in atmospheric general circulation models, Land Surface Processes in Atmospheric General Circulation Models, pp 67-108 , Edited by P.S. Eagleson. Cambridge University Press.

Charlock, T.P., and V. Ramanathan, 1985, The albedo field and cloud radiative forcing produced by a general circulation model with internally generated cloud optics, J. Atmos. Sci., 42, 1408-1429.

Clarke, R.H., 1970, Recommended methods for the treatment of the boundary layer in numerical models, Austral. Met Mag., 18, 51-73.

Cox, S.K., D.S. McDougal, D.A. Randall, and R.A. Schiffer, 1987, FIRE - The first ISCCP regional experiment, Bull. Amer. Meteorol. Soc., 68, 114-118.

Crane, R.G. and R.G. Barry 1984, The influence of clouds on climate with a focus on high latitude interactions, J. Clim., 4, 71-93.

Cunnington, W.M. and P.R. Rowntree, 1986, Simulations of the Saharan atmosphere - dependence on moisture and albedo, Q. J. R. Meteorol. Soc., 112, 971-999 .

ECMWF, 1985, Workshop on Cloud Cover Parameterization in Numerical Models, 26-28 November 1984, ECMWF, Shinfield Park, Reading, UK.

Esbensen, S.K. and Y. Kushnir, 1981, The heat budget of the global ocean, An atlas based on estimates from surface marine observations, Report No. 29, Climatic Research Institute, Oregon State University, Corvallis, Oregon, USA.

Feigelson, E.M. (Editor), 1984, Radiation in a Cloudy Atmosphere, D. Reidel Publishing Company, Dordrecht, Holland.

Foreman, S.J., 1986, Ocean and atmosphere interact! Meteorol. Mag., 115, 358-361.

Gadd, A.J., 1985, The 15-level weather prediction model, Meteorol. Mag., 114, 222-226.

Geleyn, J.F. and H.J. Preuss, 1983, A new data set of satellite-derived surface albedo values for operational use at ECMWF, Arch. Met. Geoph. Biocl., Ser. A., 32, 353-359.

Hartmann, D.L., V. Ramanathan, A. Berroir and G.E. Hunt, 1986, Earth Radiation Budget Data and Climate Research, Rev. Geophys., 24, 439-468.

Herman, G.F. and J.A. Curry, 1984, Observational and theoretical studies of solar radiation in arctic stratus clouds, J. Clim. Appl. Met., 23, 5-24.

Holland, J.Z. and E.M. Rasmusson, 1973, Measurements of the atmospheric mass, energy, and momentum budgets over a 500 kilometre square of tropical ocean, Mon. Wea. Rev., 101, 44-55.

Hsiung, J., 1985, Estimates of global oceanic meridional heat transport, J. Phys. Oceanogr., 15, 1405-1413.

Jaeger, L., 1983, Monthly and areal patterns of mean global precipitation, Variations in the Global Water Budget, D. Reidel Publishing Company.

Janowiak, J.E., A.F. Krueger, P.A. Arkin and A. Gruber, 1985, Atlas of outgoing longwave radiation derived from NOAA satellite data, NOAA atlas No. 6, National Oceanic and Atmospheric Administration, Silver Spring, Maryland, U.S.A..

Kyle, H.L., P.E. Ardanuy and E.J. Hurley, 1985, The status of the Nimbus-7 earth radiation budget data set, Bull. Amer. Met. Soc., 66, 1378-1388.

Manabe, S., 1969, Climate and the ocean circulation. I. The atmospheric circulation and the hydrology of the earth's surface, Mon. Wea. Rev., 97, 739-774.

Mitchell, J.F.B. and A. Slingo, 1988, Climatic effects of nuclear war: the role of atmospheric stability and ground heat fluxes, J. Geophys. Res., in press.

Palmer, T.N. and D.A. Mansfield, 1986, A study of wintertime circulation anomalies during past El Nino events using a high resolution general circulation model. I: Influence of model climatology, Q. J. R. Meteorol. Soc., 112, 613-638.

Palmer, T.N., G.J. Shutts and R. Swinbank, 1986, Alleviation of a systematic westerly bias in general circulation and numerical weather prediction models through an orographic gravity wave drag parametrization, Q. J. R. Meteorol. Soc., 112, 1001-1039.

Paltridge, G.W. and C.M.R. Platt, 1976, Radiative processes in meteorology and climatology, Developments in Atmospheric Science, 5, Elsevier.

Ramanathan, V., E.J. Pitcher, R.C. Malone and M.L. Blackmon, 1983, The response of a spectral general circulation model to refinements in radiative processes, J. Atmos. Sci., 40, 605-630.

Ramanathan, V., 1987, The role of earth radiation budget studies in climate and general circulation research, J. Geophys. Res., 92, 4075-4095.

Randall, D.A., J.A. Abeles, and T.G. Corsetti, 1985, Seasonal simulations of the planetary boundary layer and boundary layer stratocumulus clouds with a general circulation model, J. Atmos. Sci., 42, 641-676.

Richards, P.J.R., 1980, The parametrization of boundary layer processes in general circulation models, Ph. D. thesis, Department of Meteorology, University of Reading.

Riehl, H., 1979, Climate and weather in the tropics, Academic Press, 661 pp.

Roeckner, E., U. Schlese, J. Biercamp and P. Loewe, 1987, Cloud optical depth feedbacks and climate modelling, Nature, 329, 138-140.

Rowntree, P.R., 1984, Sensitivity of global simulations to the formulation of the evaporation of convective condensates, Workshop on convection in large-scale numerical models, pp 317-346 28 November-1 December 1983, ECMWF.

Schlesinger, M.E. and J.F.B. Mitchell, 1987, Climate model simulations of the equilibrium climatic response to increased carbon dioxide, Reviews of Geophysics, 25, 760-798.

Slingo, A., 1984, The cloudy marine boundary layer in the Meteorological Office Climate Model, Report of the WMO/CAS Expert Meeting on Atmospheric Boundary Layer Parameterization over the Oceans for Long Range Forecasting and Climate Models, Appendix I, WCP-74, WMO, Geneva.

Slingo, A., 1985a, Simulation of the earth's radiation budget with the 11-Layer general circulation model, Meteorol. Mag., 114, 121-141.

Slingo, A. (Editor), 1985b, Handbook of the Meteorological Office 11-Layer Atmospheric General Circulation Model. Volume I: Model Description, Dynamical Climatology Technical Note 29, Available on request from the Dynamical Climatology Branch, Meteorological Office, London Road, Bracknell, Berkshire.

Slingo, A., S. Nicholls and J. Schmetz, 1982, Aircraft observations of marine stratocumulus during JASIN, Q. J. R. Meteorol. Soc., 108, 833-856.

Slingo, A. and D.W. Pearson, 1987, A comparison of the impact of an envelope orography and of a parametrization of orographic gravity-wave drag on model simulations, Q. J. R. Meteorol. Soc., 113, 847-870.

Slingo, A. and J.M. Slingo, 1987, The response of a general circulation model to cloud longwave radiative forcing. I: Introduction and initial experiments, Q. J. R. Meteorol. Soc., Accepted for publication.

Slingo, A. and R.C. Wilderspin, 1985, Simulation of cloudiness with the UK Meteorological Office 11-Layer AGCM, Workshop on Cloud Cover Parameterization in Numerical Models, pp 213-231, 26-28 November 1984, ECMWF.

Slingo, A., R.C. Wilderspin and S.J. Brentnall, 1987, Simulation of the diurnal cycle of outgoing longwave radiation with an atmospheric GCM, Mon. Wea. Rev., 115, 1451-1457.

Slingo, J.M., 1980, A cloud parametrization scheme derived from GATE data for use with a numerical model, Q. J. R. Meteorol. Soc., 106, 747-770.

Slingo, J.M., 1982, A study of the earth's radiation budget using a general circulation model, Q. J. R. Meteorol. Soc., 108, 379-405.

Slingo, J.M., 1987, The development and verification of a cloud prediction scheme for the ECMWF model, Q. J. R. Meteorol. Soc., 113, 899-927.

Stephens, G.L., G.W. Paltridge and C.M.R. Platt, 1978, Radiation profiles in extended water clouds. III: Observations, J. Atmos. Sci., 35, 2133-2141.

Stephens, G.L. and P.J. Webster, 1981, Clouds and climate: Sensitivity of simple systems, J. Atmos. Sci., 38, 235-247.

Tiedtke, M., 1984, The sensitivity of the time-mean large-scale flow to cumulus convection in the ECMWF model, Workshop on convection in large-scale numerical models, 28 November-1 December 1983, ECMWF.

Tiedtke, M., W.A. Heckley and J.M. Slingo, 1988, Tropical forecasting at ECMWF: On the influence of physical parametrization on the mean structure of forecasts and analyses, Q. J. R. Meteorol. Soc., 114, In press.

Warren, S.G., C.J. Hahn, J. London, R.M. Chervin and R.L. Jenne, 1986: Global distribution of total cloud cover and cloud type amounts over land, NCAR Technical Note NCAR/TN-273+STR.

Warrilow, D.A., 1986, The sensitivity of the UK Meteorological Office atmospheric general circulation model to recent changes to the parametrization of hydrology, proceedings of the ISLSCP Conference, Rome, Italy, 2-6 December 1985, pp 143-149, ESA SP-248.

Warrilow, D.A., A.B. Sangster and A. Slingo, 1986, Modelling of land surface processes and their influence on European Climate, Dynamical Climatology Technical Note 38, Meteorological Office, Bracknell.

Weare, B.C., P.T. Strub and M.D. Samuel, 1981, Annual mean surface heat fluxes in the tropical Pacific Ocean, J. Phys. Oceanogr., 11, 705-717.

Welch, R.M., S.K. Cox and J.M. Davis, 1980, Solar Radiation and Clouds, Meteorol. Mon., 17, No. 39.

Wetherald, R.T., and S. Manabe, 1986, An investigation of cloud cover change in response to thermal forcing, Climatic Change, 8, 5-23.

Wilson, C.A. and J.F.B. Mitchell, 1987, A 2 x CO_2 climate sensitivity experiment with a global climate model including a simple ocean, J. Geophys. Res., 92, 13315-13343.

Wilson, M.F., 1984, The construction and use of land surface information in a general circulation climate model, Ph. D. Thesis, University of Liverpool.

Wilson, M.F. and A. Henderson-Sellers, 1985, A global archive of land cover and soils data for use in general circulation climate models, J. Clim., 5, 119-143.

FIGURE CAPTIONS

Figure 1 Outgoing Longwave Radiation (OLR) in Wm^{-2} for the northern summer season (June to August) for (a) the summer of 1979, derived from Nimbus 7 Narrow Field of View data, (b) the initial integration with interactive cloud and (c) the integration of the new model. The contour interval is 25 Wm^{-2} and values below 225 Wm^{-2} are stippled.

Figure 2 Total precipitation (rain plus snow) for the northern summer season for (a) the data of Jaeger (1983), (b) the initial integration and (c) the integration of the new model. The contours are at 0.1,1,2,5, 10 and 20 mm/day and values above 5 mm/day are stippled.

Figure 3 As Figure 1 but for shortwave planetary albedo, expressed as a percentage. The contour interval is 10% with values above 30% shown stippled.

Figure 4 (a) Low cloud amount and (b) Convective cloud amount, expressed as a fraction, for the northern summer season from the initial integration. The contour interval for low cloud is 0.2 with values above 0.5 stippled. For convective cloud the contour interval is 0.05 with values above 0.2 stippled.

Figure 5 Annual-mean net surface heating (shortwave heating minus longwave cooling minus upward sensible and latent heat fluxes) from (a) the estimates by Esbensen and Kushnir (1981), (b) one year of the initial integration and (c) four years from the integration of the new model. The contour interval is 20Wm^{-2} with negative areas (i.e. net surface cooling) stippled.

Figure 6 Tephigrams of the temperature T and dew-point temperature T_d (a) obtained during BOMEX (Holland and Rasmusson 1973), (b) for the model grid-point at 16.25° N 54.375° W for the northern summer season from the initial integration (c) for the same grid-point and season from the integration of the new model and (d) for the same grid-point and season from the integration of the new model but without the split final detrainment change to the convection scheme.

On this thermodynamic diagram, isobars are nearly horizontal and are labelled every 100mb. Isotherms are straight lines sloping upwards to the right and are labelled every 10°C. The steeper dashed lines are of constant humidity mixing ratio, labelled at the bottom of each panel. Dry adiabats are drawn orthogonal to the isotherms and meet them at 1000mb, from which point the curved moist adiabats are also drawn and labelled every 10°C.

Figure 7 The diagram on the left is a schematic tephigram of the profiles of temperature T and dew-point temperature T_d in the trade-wind region, with the model grid points shown. On the right, the evolution of a buoyant parcel from the lowest model layer is illustrated for the original convection scheme and the modified version. Entrainment into and detrainment out of the parcel are represented by the horizontal arrows. In the original scheme, the parcel fails the test for buoyancy in layer k - 1 and detrains completely in layer k, within the atmospheric boundary layer. In the modified scheme, the final detrainment is split between layers k and k - 1, so that some modification of the air above the inversion occurs.

Figure 8 (a) Low cloud amount, expressed as a fraction, for the northern summer season from the integration of the new model. The contour interval is 0.2 with the first contour at 0.1 and values above 0.5 stippled.

(b) Boundary layer depth (m) at 00 hours GMT for the northern summer season from the integration of the new model. The contour interval is 250 m and values below 250 m are stippled.

Figure 9 (a) Total precipitation, (b) Low cloud amount and (c) Shortwave planetary albedo for the northern summer seas(k from the integration of the new model but without the split final detrainment change to the convection scheme. The contouring and shading are the same as in previous figures.

Figure 10. (a) High cloud amount and (b) Medium cloud amount, expressed as a fraction, for the northern summer season from the integration of the new model. The contour interval in both cases is 0.2 with the first contour at 0.1 and values above 0.5 stippled.

Figure 11 (a) Convective cloud amount, expressed as a fraction, for the northern summer season from the integration of the new model. The contour interval is 0.05 and values above 0.2 are stippled.

(b) Convective cloud top pressure (mb). The contour interval is 100 mb and values less than 400 mb are stippled.

Figure 12 Latitude-pressure cross section of the zonally-averaged fractional amounts of layer cloud for the northern summer season from the integration of the new model. The contour interval is 0.05 and values above 0.15 are stippled.

Figure 13 Outgoing Longwave Radiation (OLR) in W m^{-2} for the northern winter season (December to February) for (a) the winter of 1979/1980 derived from Nimbus 7 Narrow Field of View data and (b) the integration of the new model. The contour interval is 25 W m^{-2} and values below 225 W m^{-2} are stippled.

Figure 14 As Figure 13 but for shortwave planetary albedo, expressed as a percentage. The contour interval is 10% with values above 30% shown stippled.

TABLE 1. Cloud radiative properties assumed for the initial integration with interactive cloud.

Cloud	Shortwave			Longwave
Type	Reflectivity	Transmissivity	Absorptivity	Emissivity
Low	0.6	0.3	0.1	1.0
Medium	0.6	0.3	0.1	1.0
High	0.2	0.75	0.05	0.75
Convective	0.6	0.3	0.1	1.0

TABLE 2. Surface shortwave albedos assumed for the initial integration with interactive cloud.

Surface type	Albedo	Comments
Sea	0.06	
Sea-ice	0.8	$T_S < 268K$
	$0.5 + 0.06\ (273 - T_S)$	$268K \leq T_S \leq 273K$
		T_S is surface temperature*
Land-ice	0.8	
Snow-free land	α_L depends on land type	See text
Snow-covered land	$\alpha_S = \alpha_L + 0.38\ (\text{Snowdepth})^{0.5}$	Snowdepth is in cm
	But $\alpha_S \geq 0.6$	of water equivalent

*The expressions for sea-ice are those which were programmed into the model. However, the surface temperature for sea-ice was constrained to be less than 271.2K, so the minimum obtainable surface albedo was actually 0.608 rather than 0.5.

TABLE 3. CHANGES TO CREATE THE NEW VERSION OF THE 11-LAYER MODEL.

	CHANGE	REASON FOR IMPLEMENTATION
a.	Shallow convection: "Split final detrainment".	To simulate effects of shallow cumulus convection.
b.	Calculation of convective cloud cover:	
	1) from convection scheme used by rest of model.	See Section 3b.
	2) amounts calculated from parcel liquid water path.	Takes advantage of item h.
c.	New boundary-layer scheme ("Richards").	Allows boundary layer to vary in depth, and an improved representation of sub-tropical Sc.
d.	Revised treatment of layer cloud :	
	1) Cloud predicted in all layers except top.	Generalisations required for climate change and sensitivity experiments.
	2) Latitudinal dependence removed.	To tune global averages.
	3) Revised relative humidity thresholds.	See Section 3e.
e.	Surface albedos increased over the Sahara.	See Section 3f.
f.	Emissivity of high cloud reduced from 0.75 to 0.6	See Section 3g.
g.	Revised albedos for sea-ice.	
h.	Convection scheme:	
	1) Changes to treatment of detrainment.	Removes arbitrary features from original scheme.
	2) Revised treatment of precipitation formation.	From experience with the scheme in the Met. Office operational NWP model.
	3) Revised treatment of evaporation of precipitation.	See Section 3h.
i.	New land surface model:	
	1) 4-layer soil temperature scheme.	Improves surface temperature response to external forcing
	2) Hydrology scheme	More realistic treatment of soil moisture and runoff.
j.	Evaporation of large-scale precipitation included.	For consistency with convection scheme.
k.	Orographic gravity-wave drag parametrization	Slingo and Pearson (1987)
l.	New SSTs and sea-ice distributions.	New compilation for 1951-1980.
m.	PMSL filtered every 10 days.	To remove roughnesses in height fields.
	Various program errors corrected.	Obvious.

The letters refer to the corresponding sub-sections in Section 3.

TABLE 4. Brief specification of the new version of the 11-Layer Model

1.	Global, primitive equation model.
2.	2.5 x 3.75 degree latitude/longitude grid (72 x 96 points).
3.	11 sigma layers with boundaries at 1.0, 0.975, 0.9, 0.79, 0.65, 0.51, 0.37, 0.27, 0.195, 0.125, 0.06 and 0.0.
4.	Variables: surface pressure and 11 x (u,v,T,q).
5.	Second order, energy-conserving finite difference scheme. 10 minute leapfrog timestep.
6.	Computational stability controlled by East-West multipoint filtering near poles. Grid-point noise damped by non-linear horizontal diffusion. PMSL filtered every 10 days.
7.	Dynamical equations are in flux form and include virtual temperature effects.
8.	Mean orography plus orographic gravity wave drag scheme.
9.	Land surface: New 4-layer soil temperature model. New hydrology model. Interactive snow cover and soil moisture.
10.	Stability-dependent surface exchange coefficients.
11.	Ekman-layer fluxes: Eddy diffusivity approach. Boundary layer can be up to three layers deep.
12.	Penetrative convection scheme, using parcel theory modified by entrainment and detrainment. Valid for both dry and moist convective processes.
13.	Large-scale precipitation scheme.
14.	Interactive radiation and diagnostic cloud schemes, called every 3 hours of model time. Fractional cover of layer clouds (amounts from relative humidity) and convective clouds (amounts from parcel liquid water paths calculated in convection scheme).

a) OLR from Nimbus 7 (JJA)

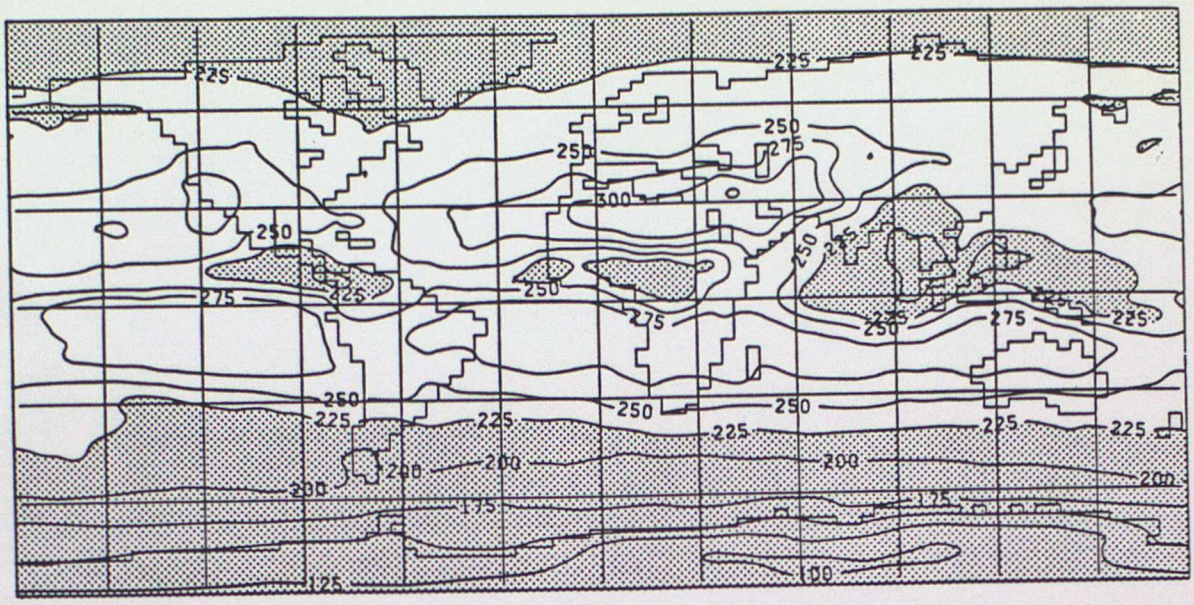

b) OLR from initial integration (JJA)

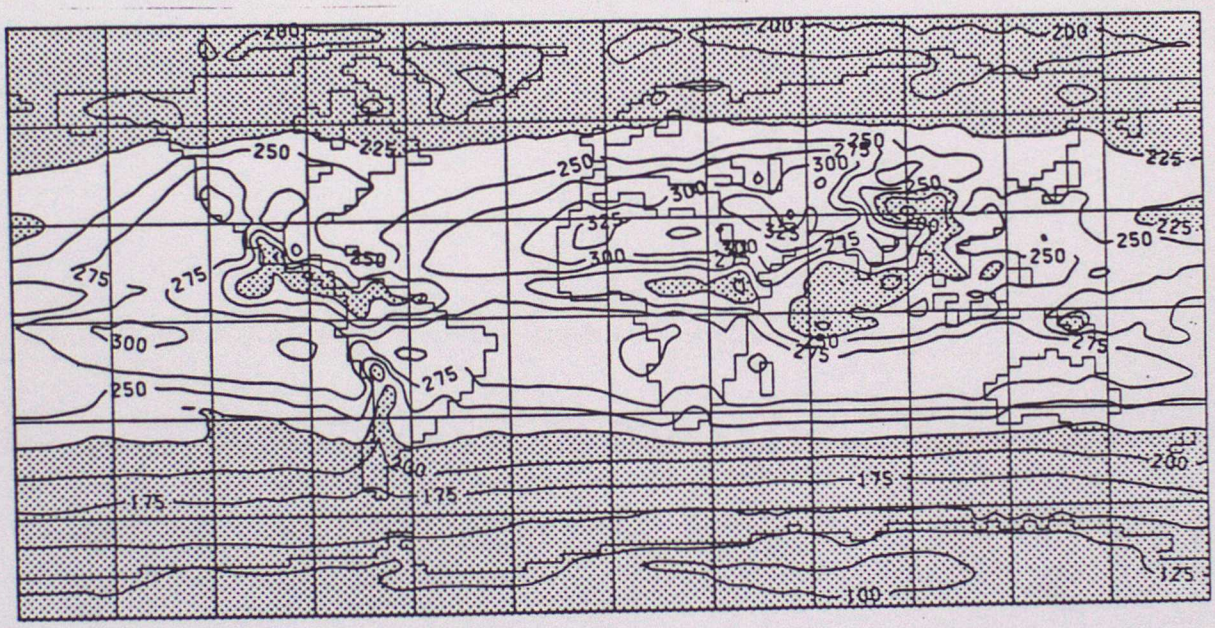

c) OLR from new model (JJA)

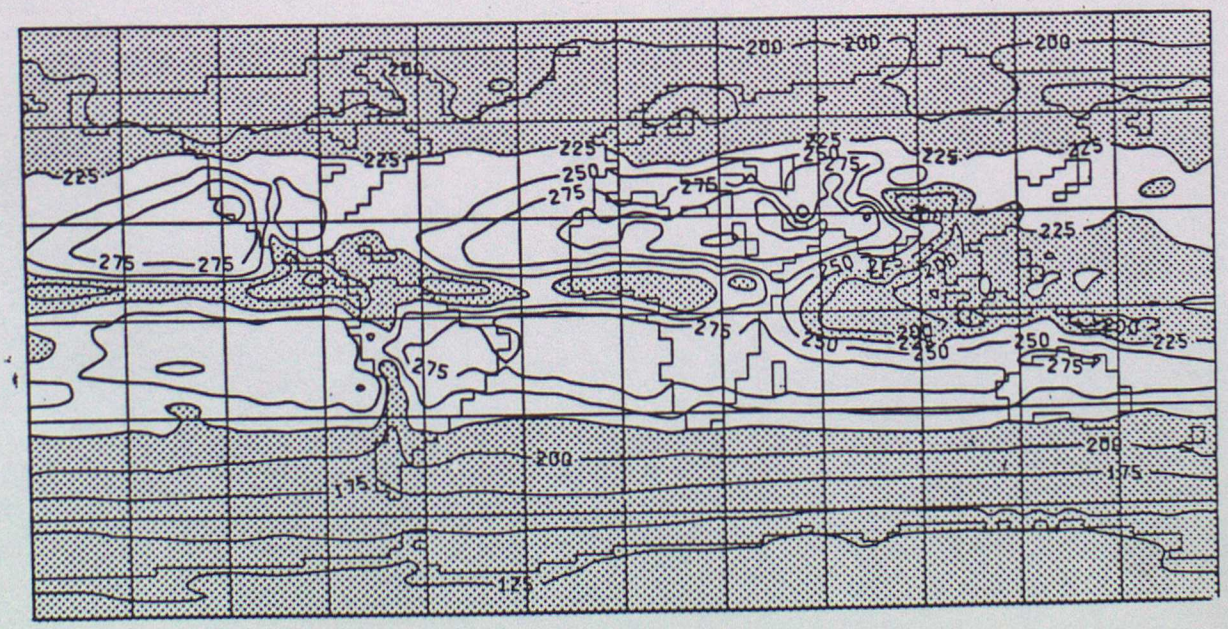

Figure 1

a) Total precipitation (mm/day) from Jaeger (JJA)

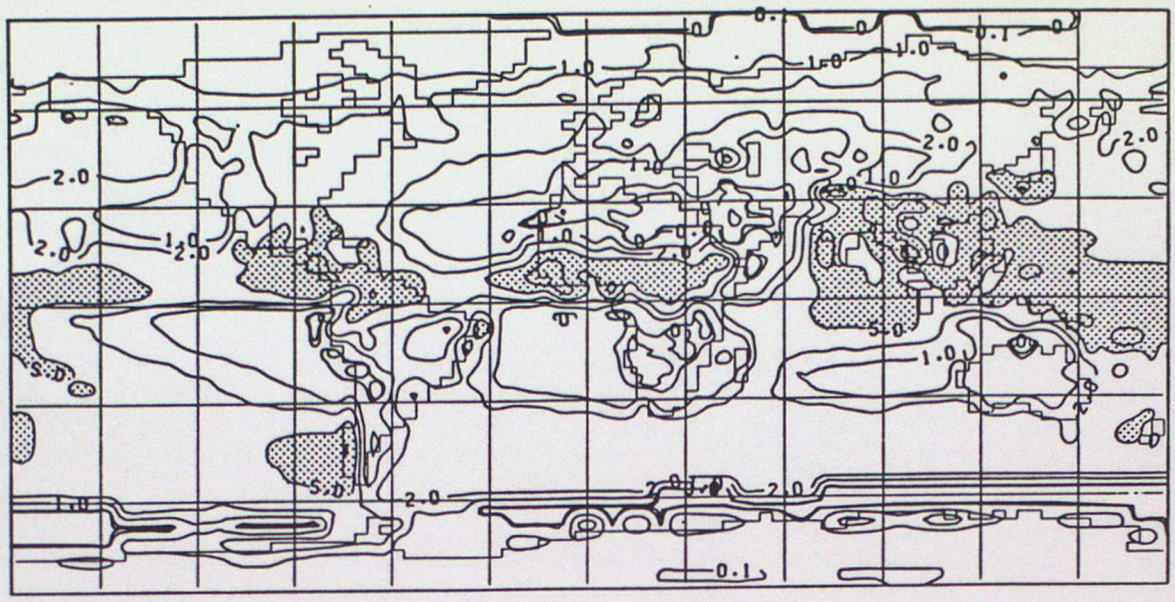

b) Total precipitation (mm/day) from initial integration (JJA)

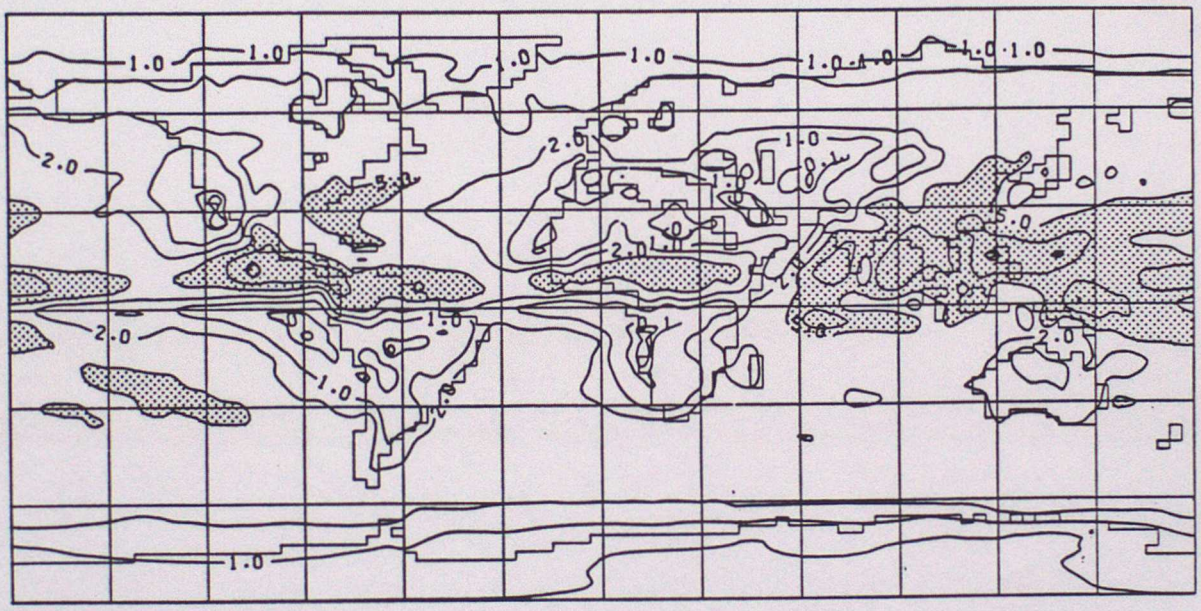

c) Total precipitation (mm/day) from new model (JJA)

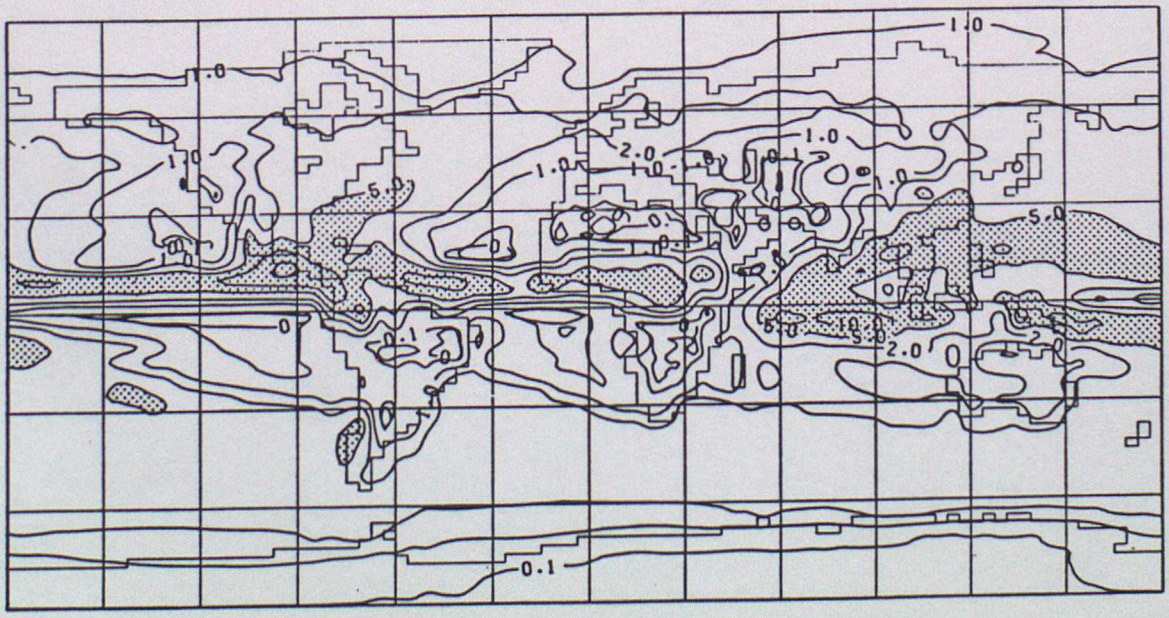

Figure 2

a) Shortwave albedo (percent) from Nimbus 7 (JJA)

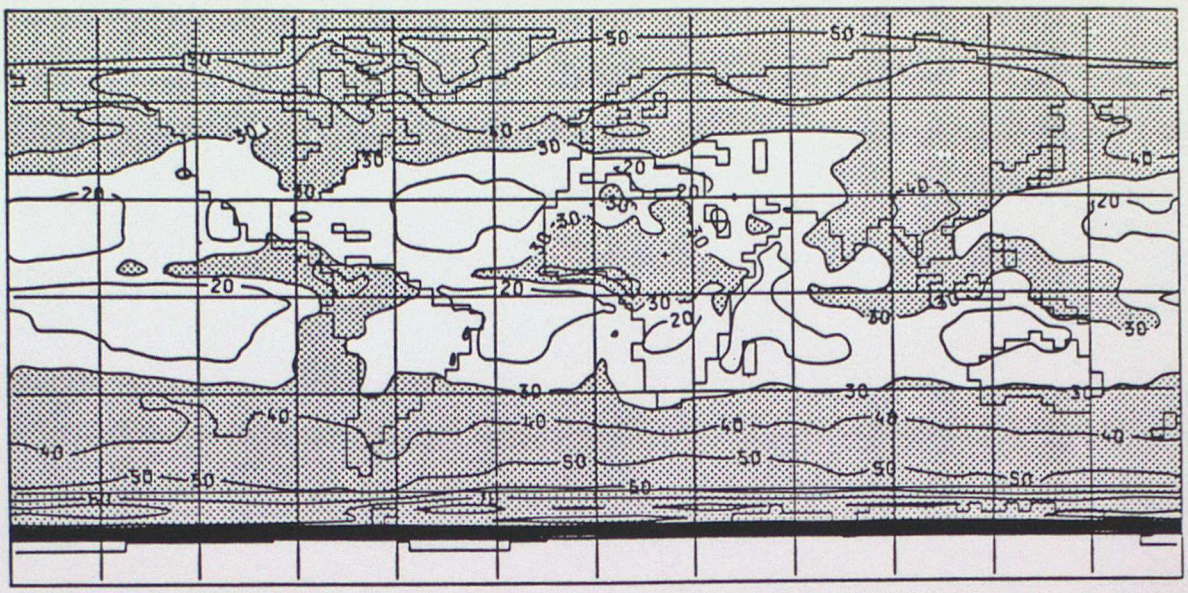

b) Shortwave albedo (percent) from initial integration (JJA)

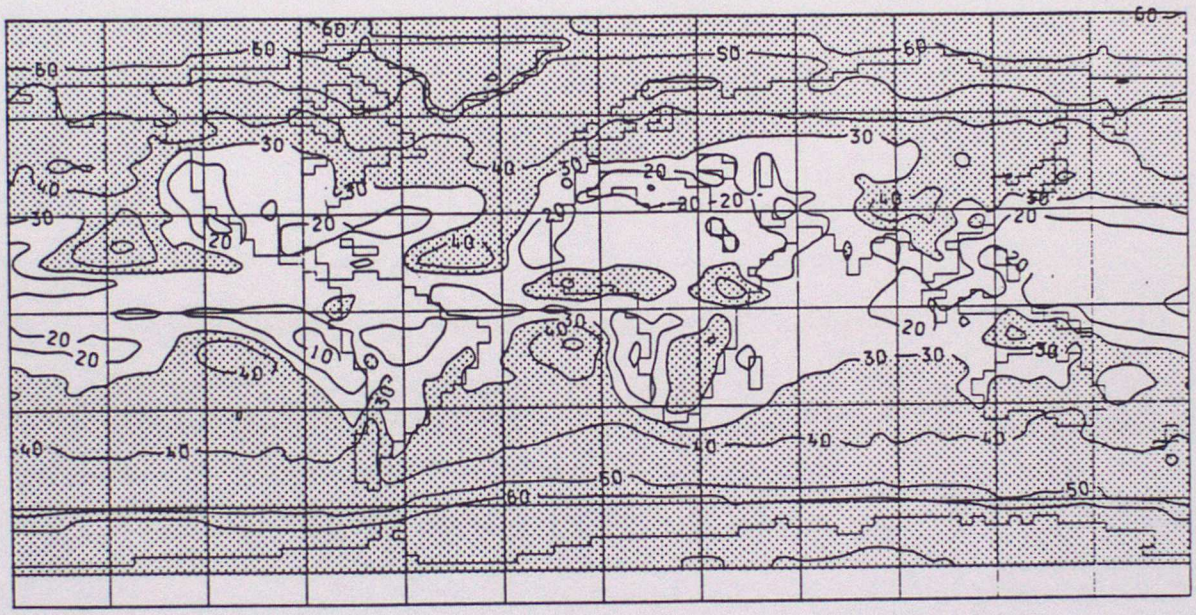

c) Shortwave albedo (percent) from new model (JJA)

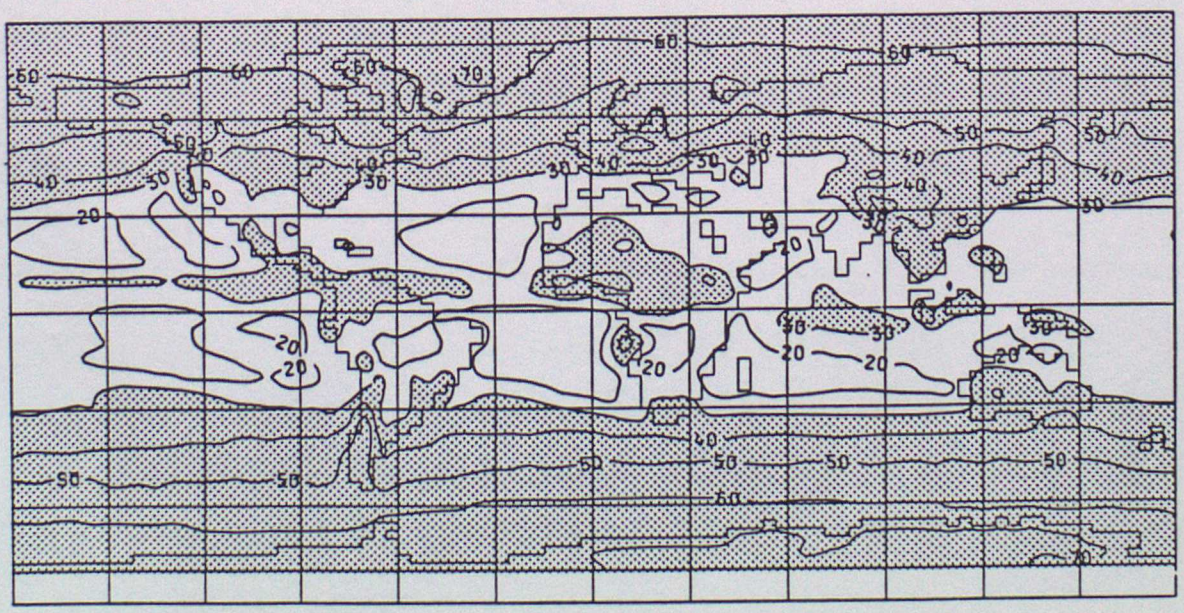

Figure 3

a) Low cloud fraction from initial integration (JJA)

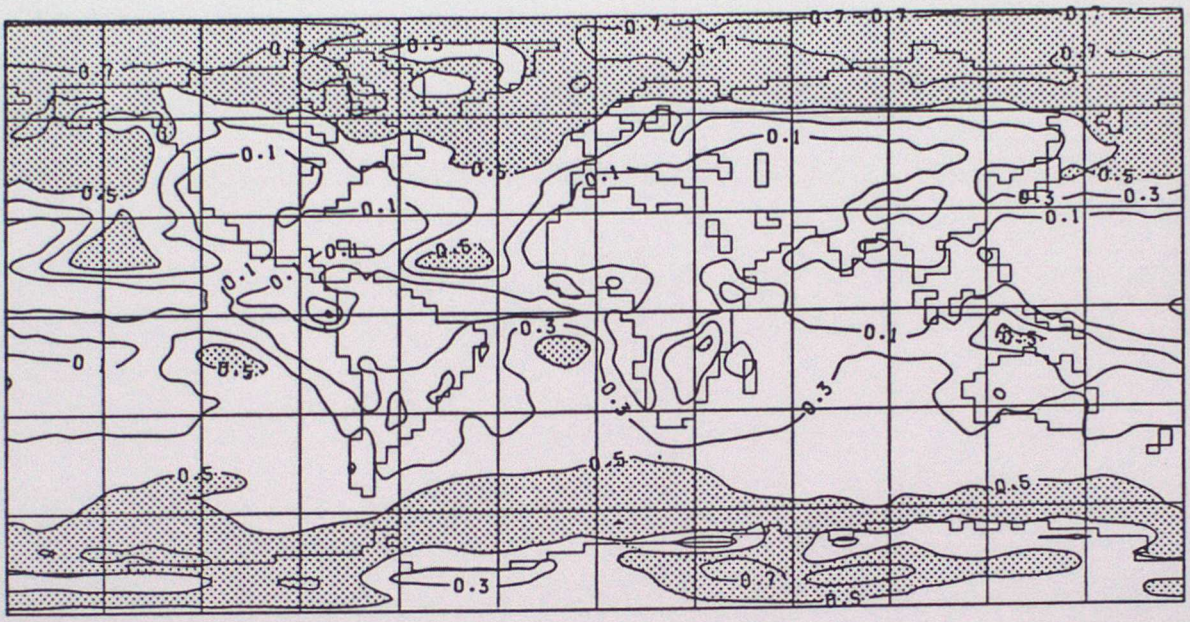

b) Convective cloud fraction from initial integration (JJA)

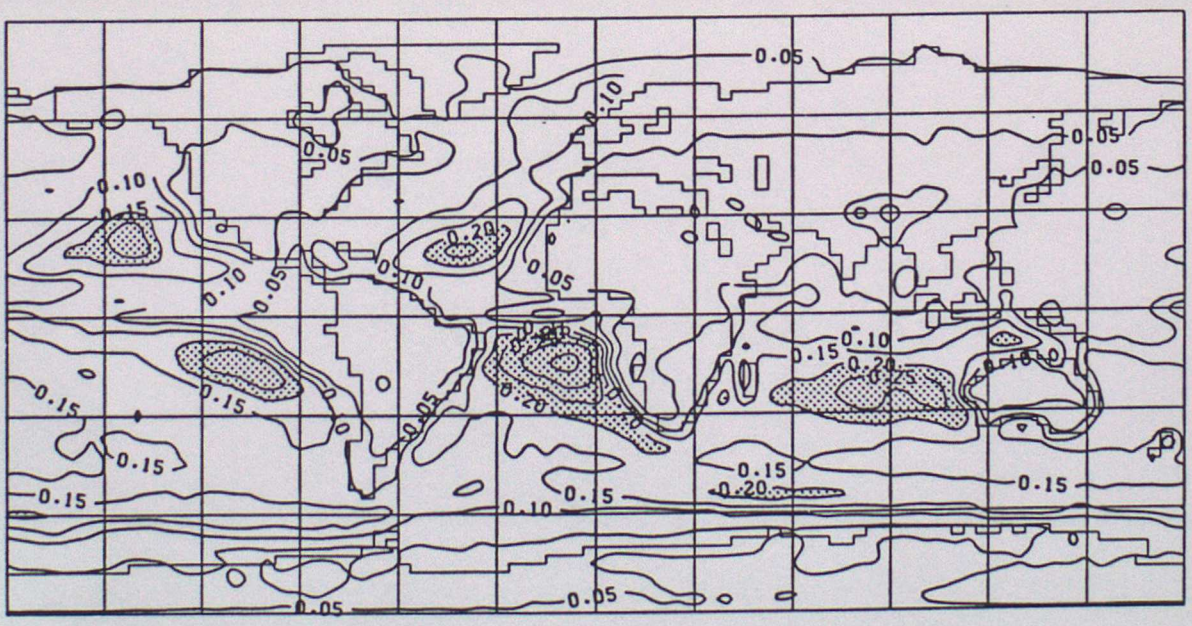

Figure 4

a) Annual-mean net surface heating (W m^{-2}) from Esbensen & Kushnir

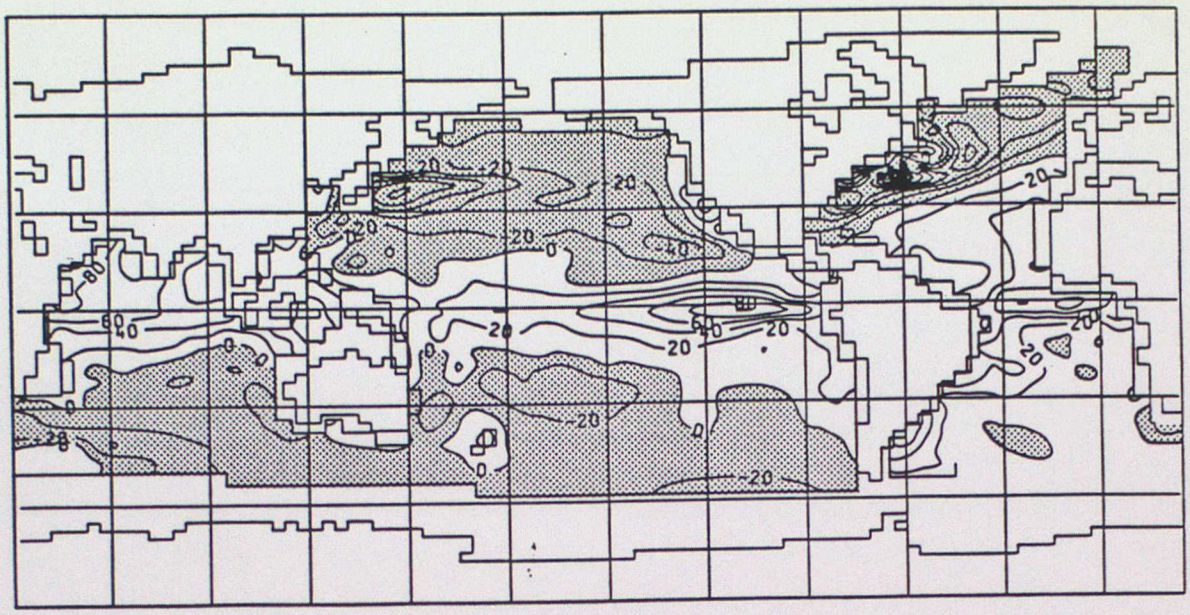

b) Annual-mean net surface heating (W m^{-2}) from initial integration

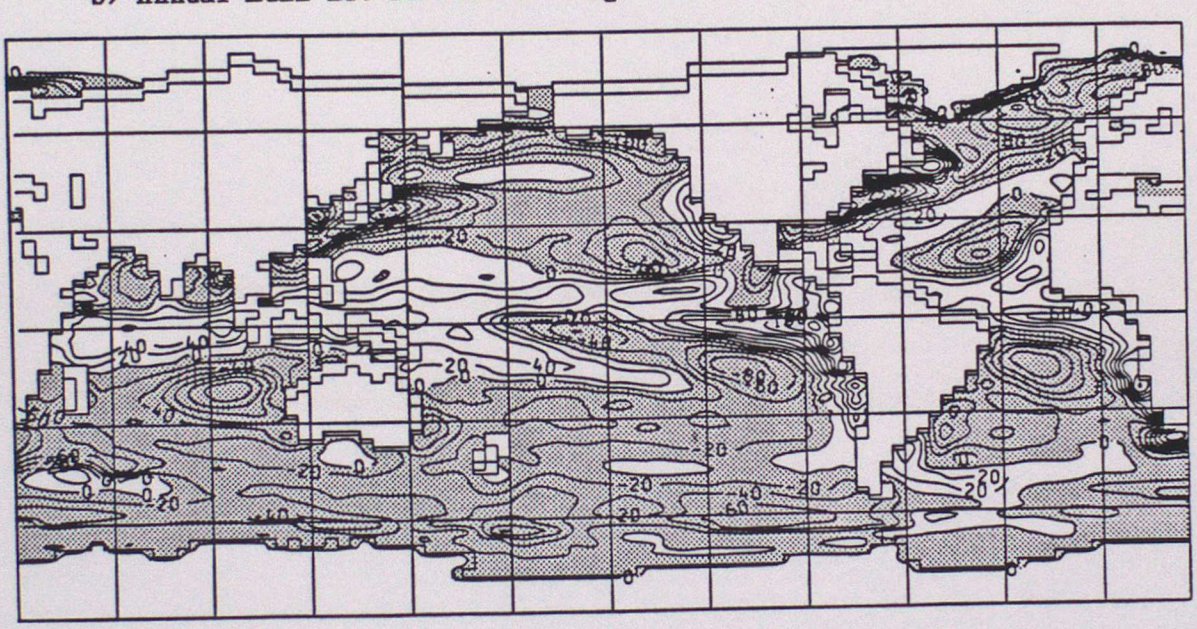

c) Annual-mean net surface heating (W m^{-2}) from new model

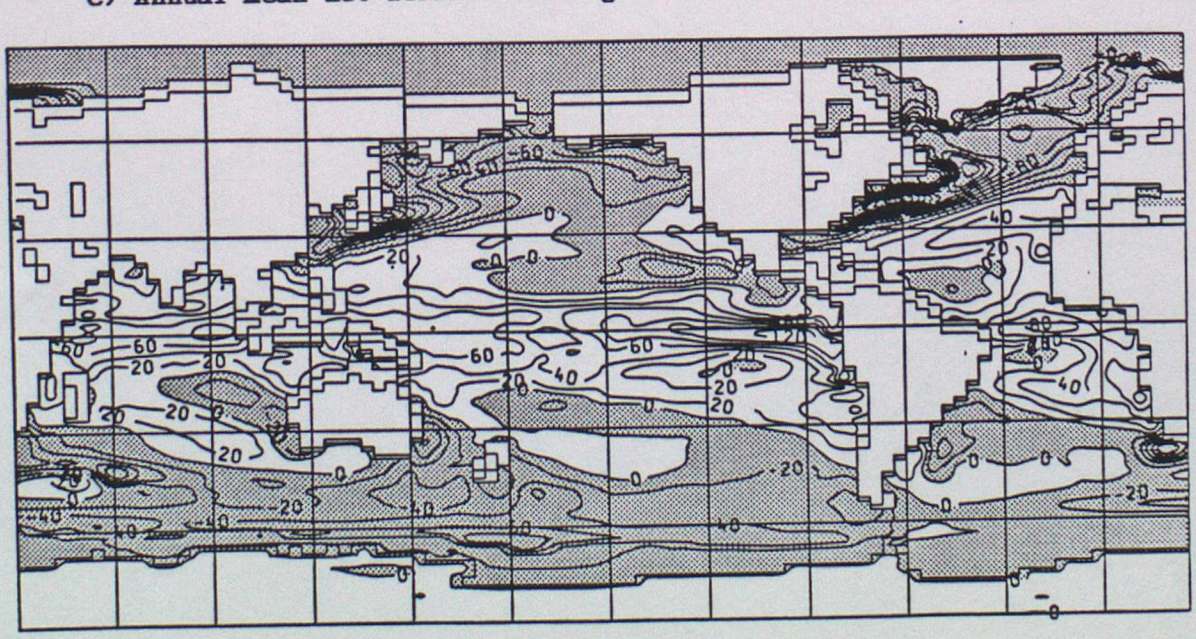

Figure 5

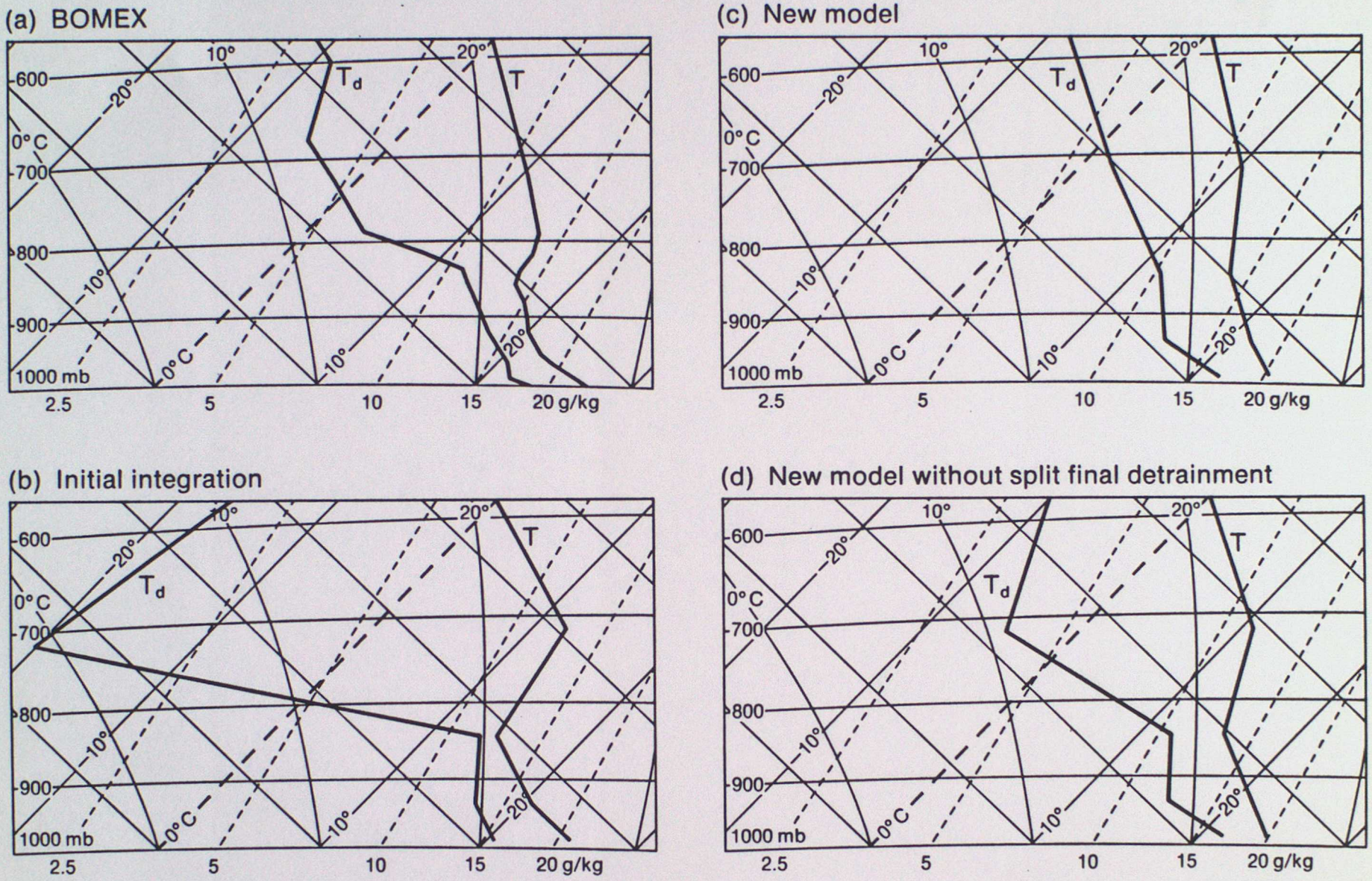
(a) BOMEX
(c) New model
(b) Initial integration
(d) New model without split final detrainment
600
700
800
900
1000 mb
0° C
10°
20°
T_d
T
2.5
5
10
15
20 g/kg

Figure 6

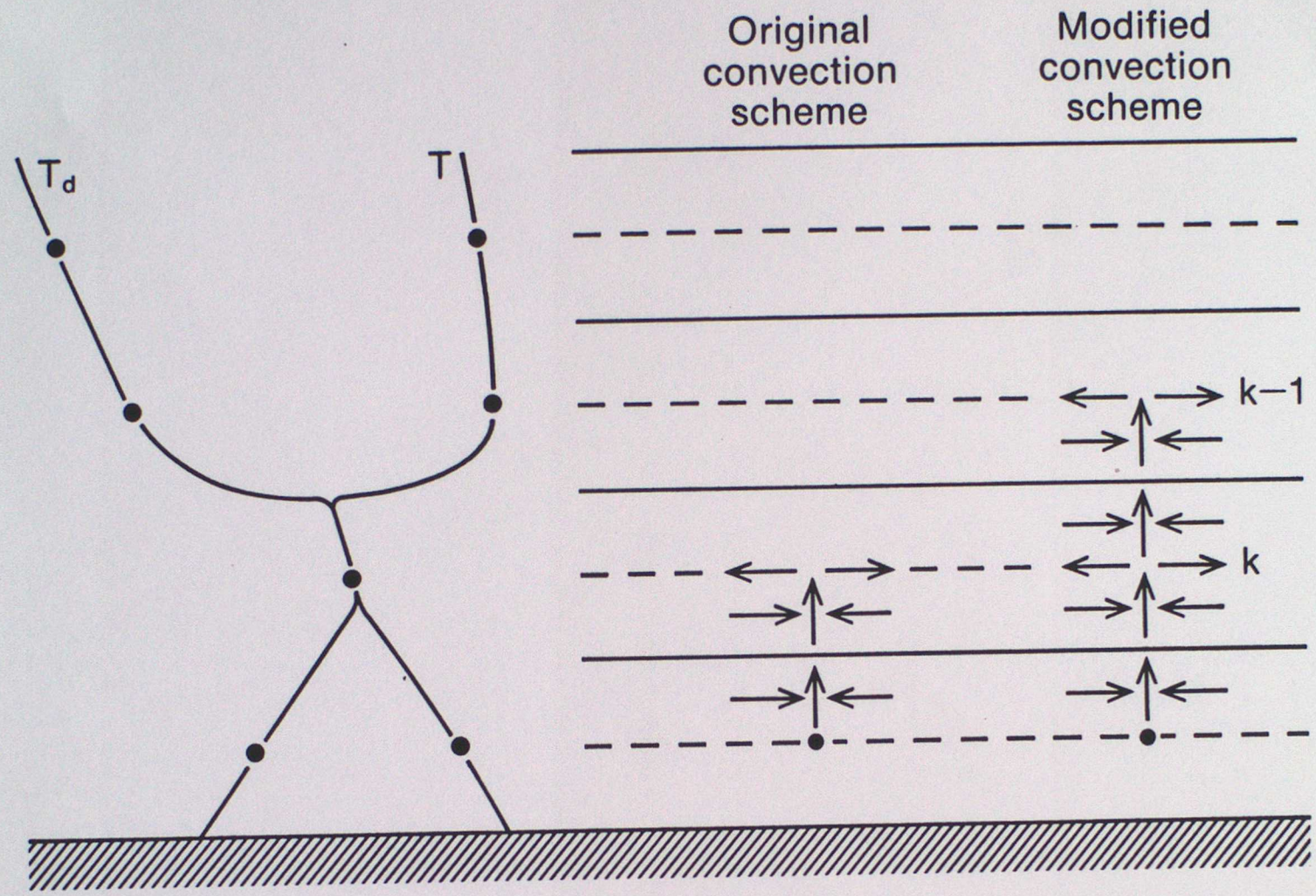
Original convection scheme
Modified convection scheme
T_d
T
k−1
k

Figure 7

a) Low cloud fraction from new model (JJA)

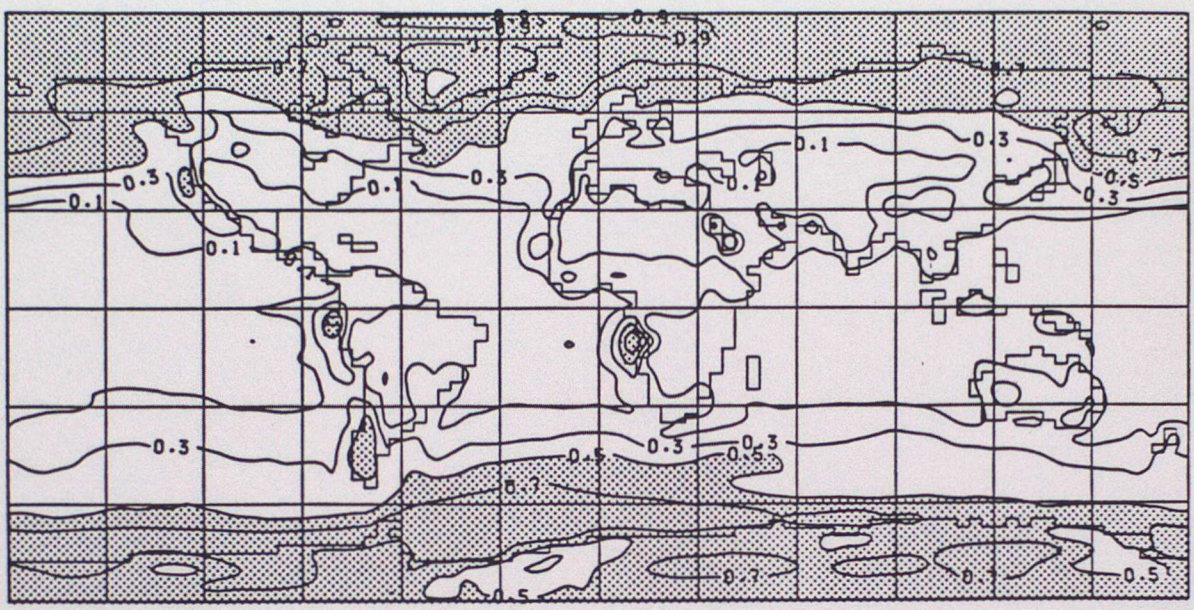

b) Boundary layer depth (m) from new model (JJA)

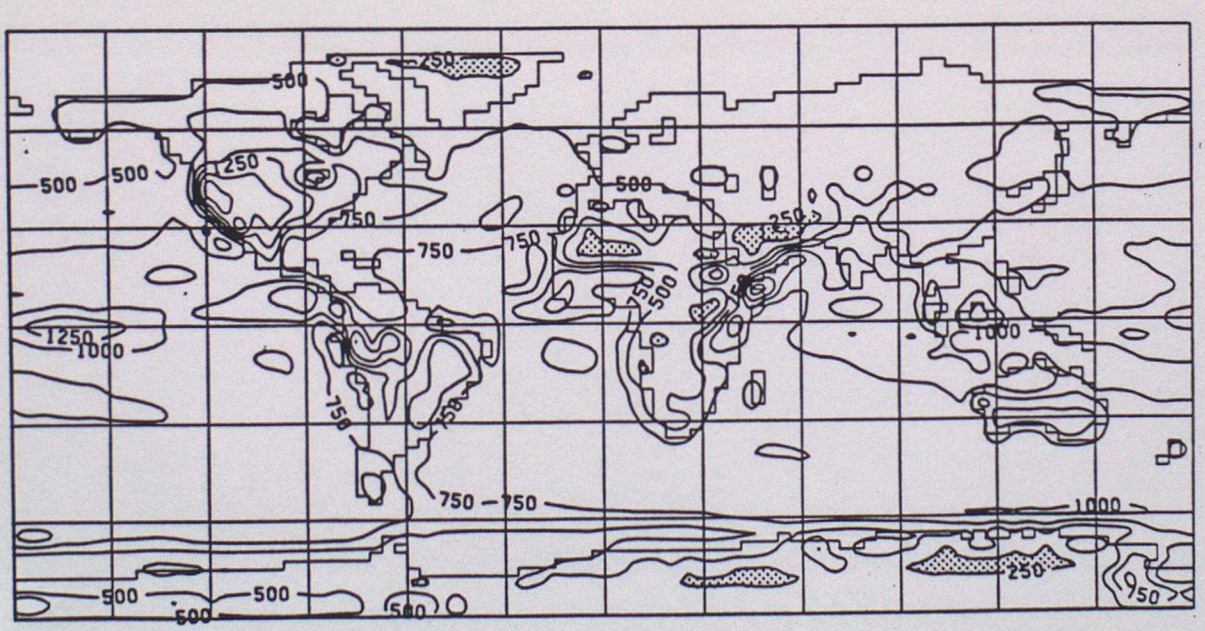

Figure 8

a) Total precipitation (mm/day) from experiment RSFD (JJA)

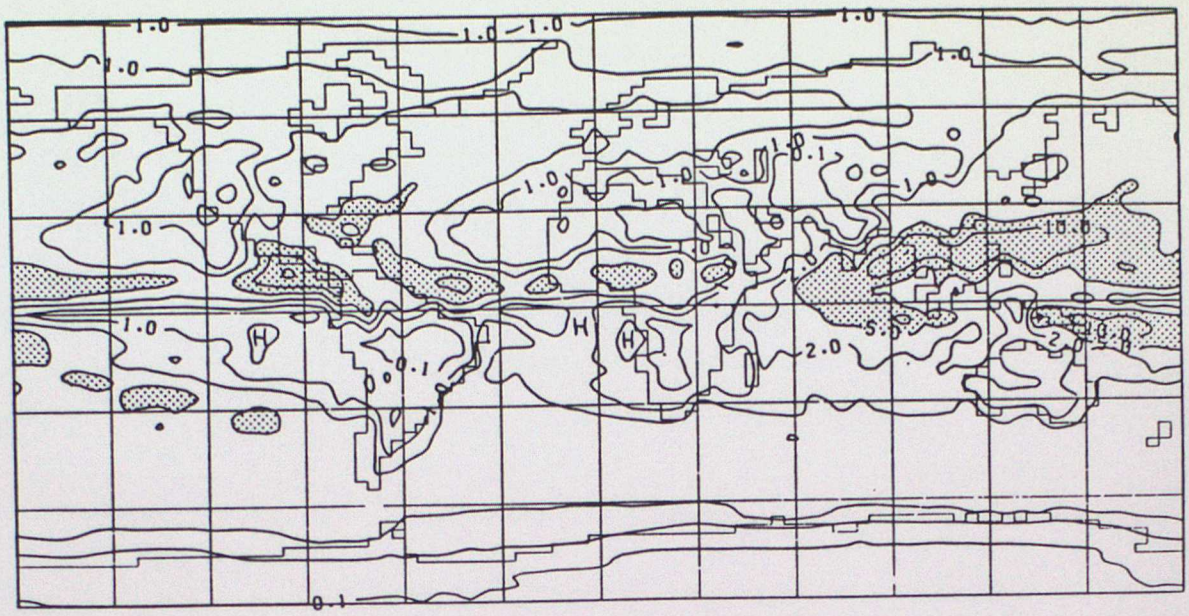

b) Low cloud fraction from experiment RSFD (JJA)

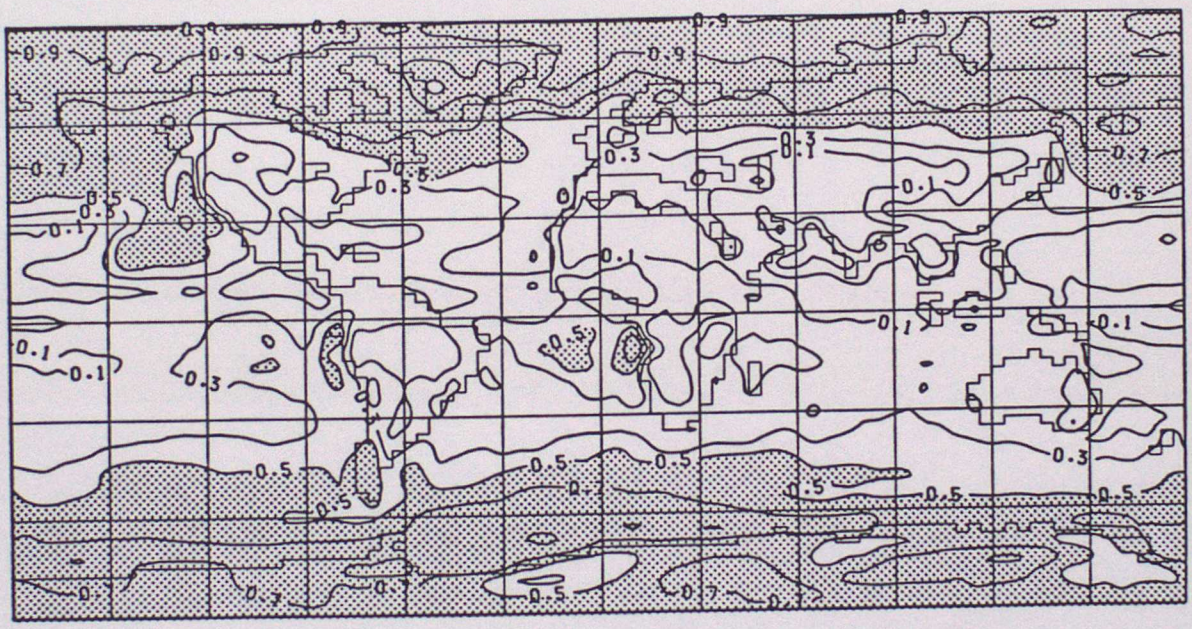

c) Shortwave albedo (percent) from experiment RSFD (JJA)

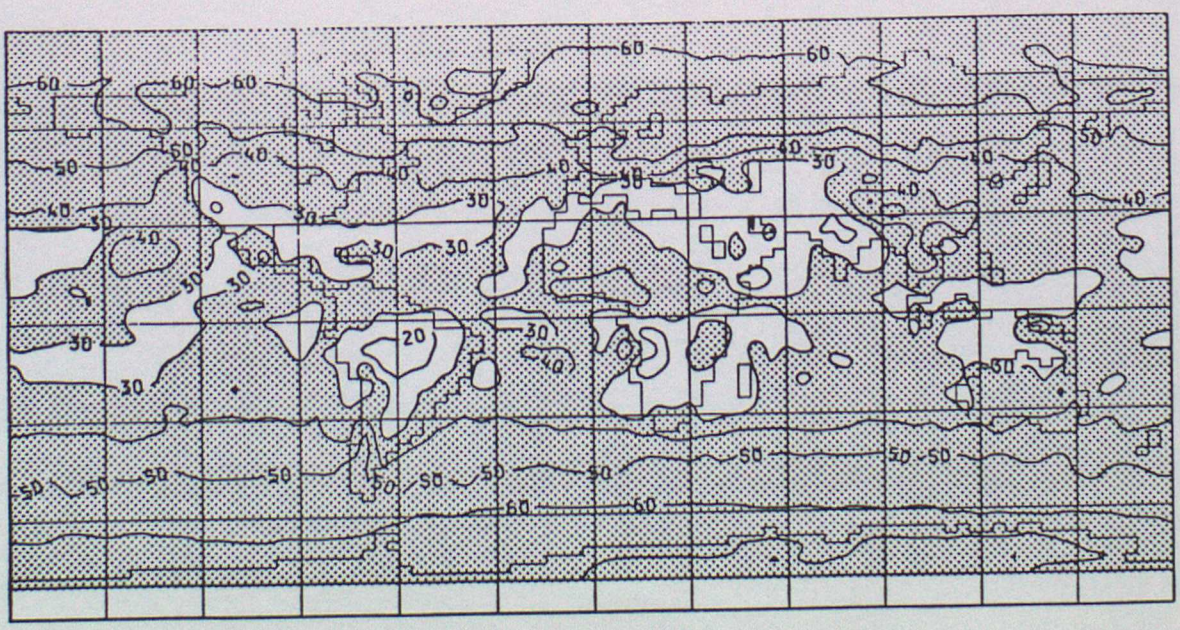

Figure 9

a) High cloud fraction from new model (JJA)

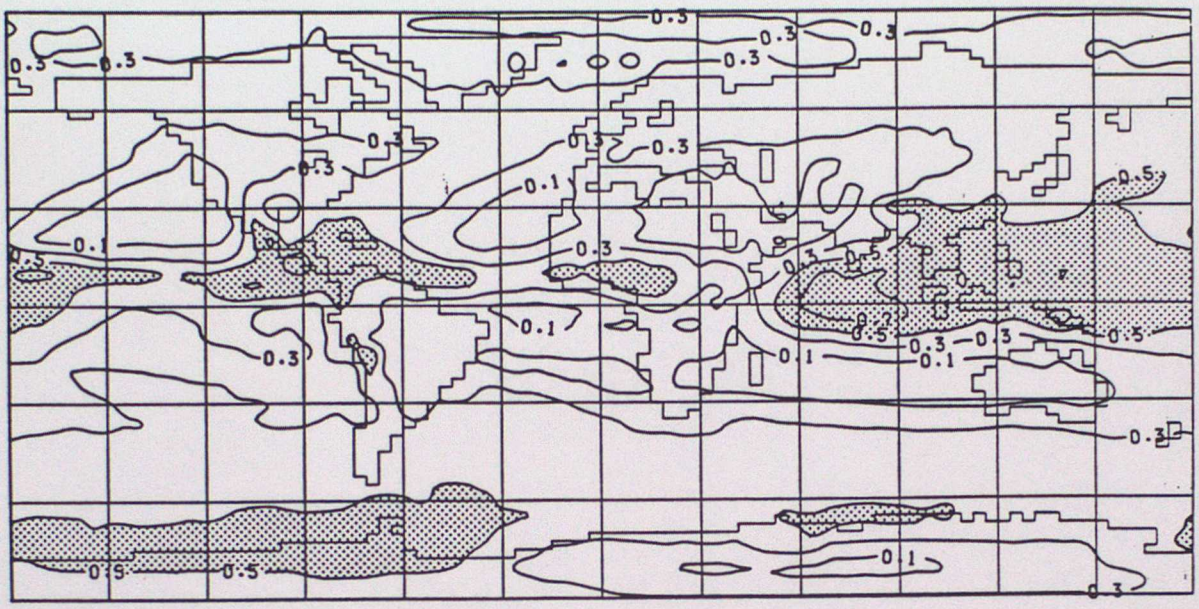

b) Medium cloud fraction from new model (JJA)

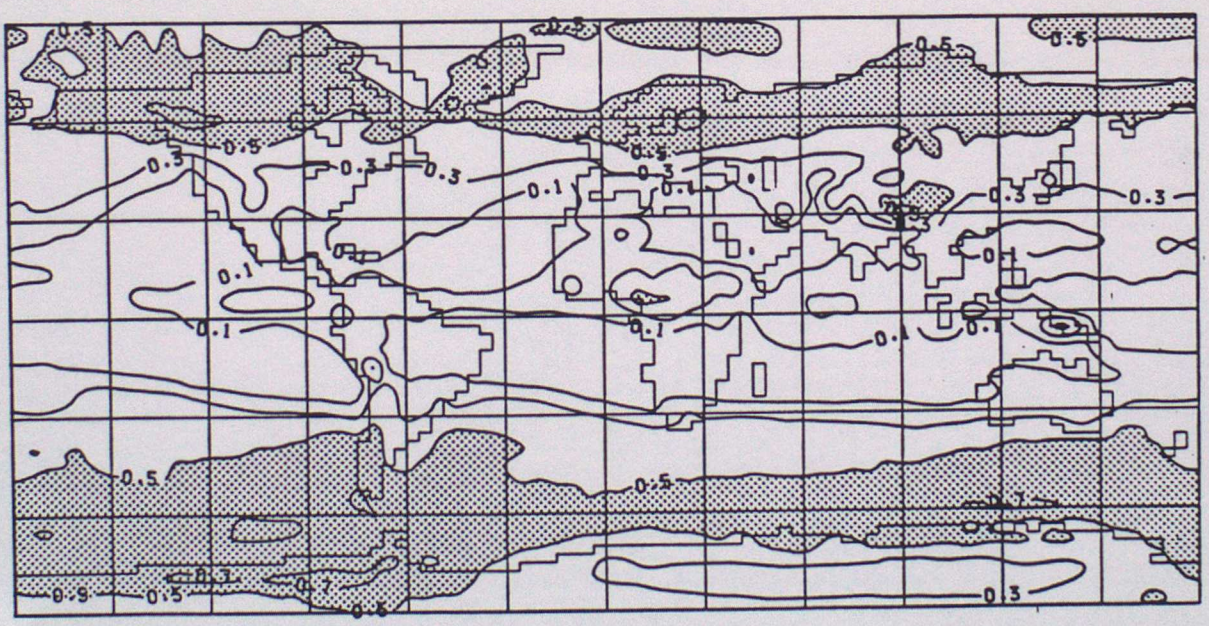

Figure 10

a) Convective cloud fraction from new model (JJA)

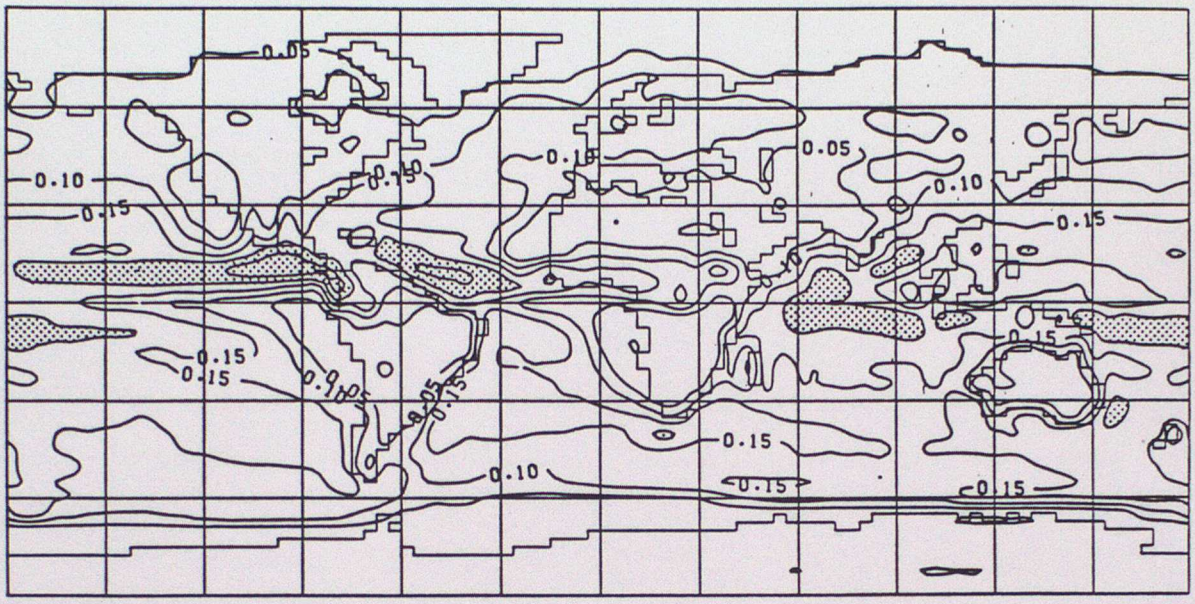

b) Convective cloud top pressure (mb) from new model (JJA)

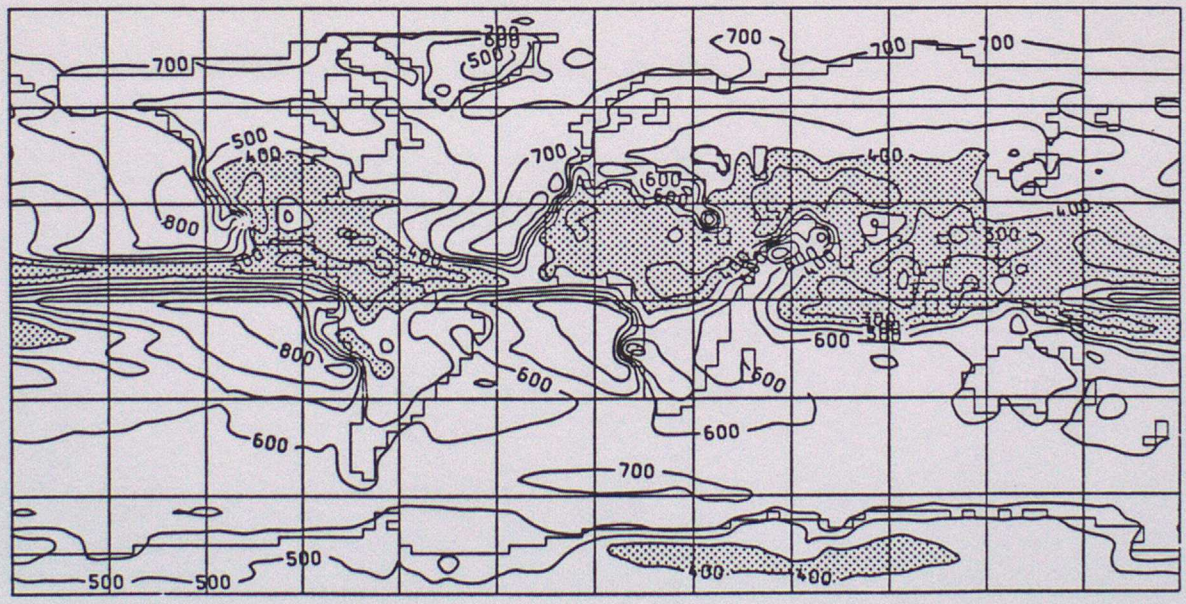

Figure 11

Zonal-average layer cloud fraction from new model (JJA)

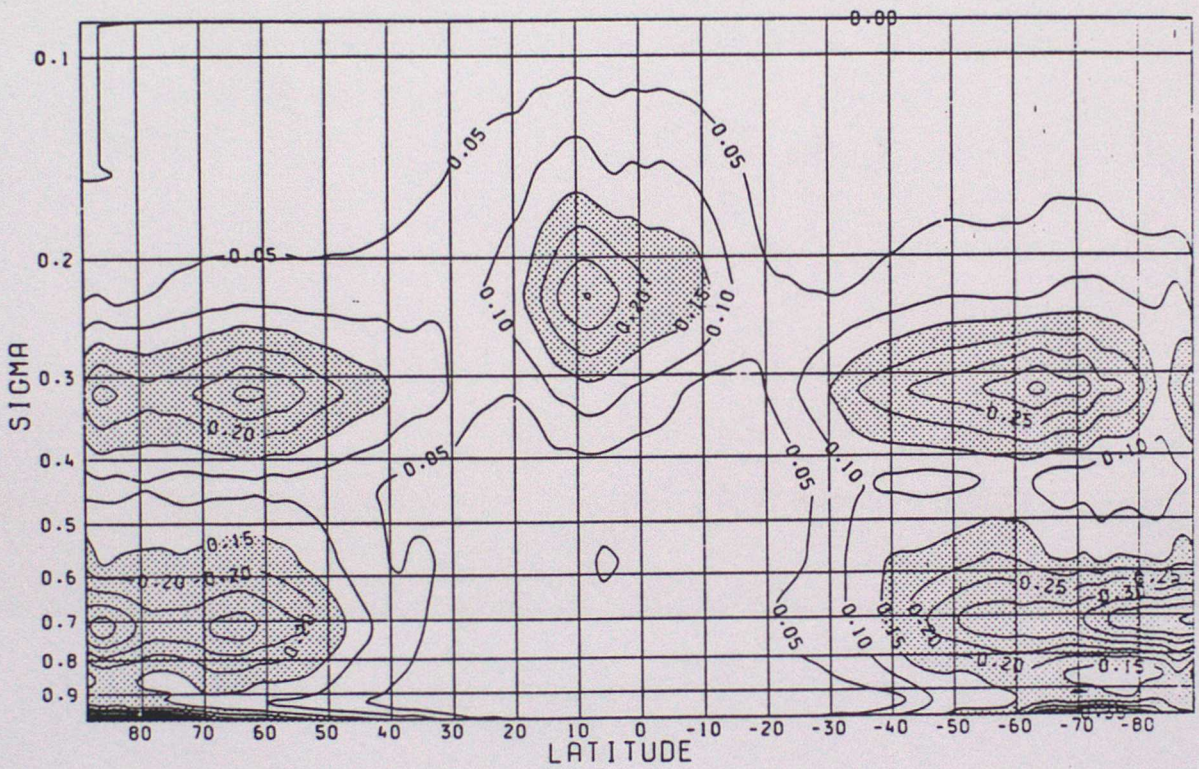

Figure 12

a) OLR (W m^{-2}) from Nimbus 7 (DJF)

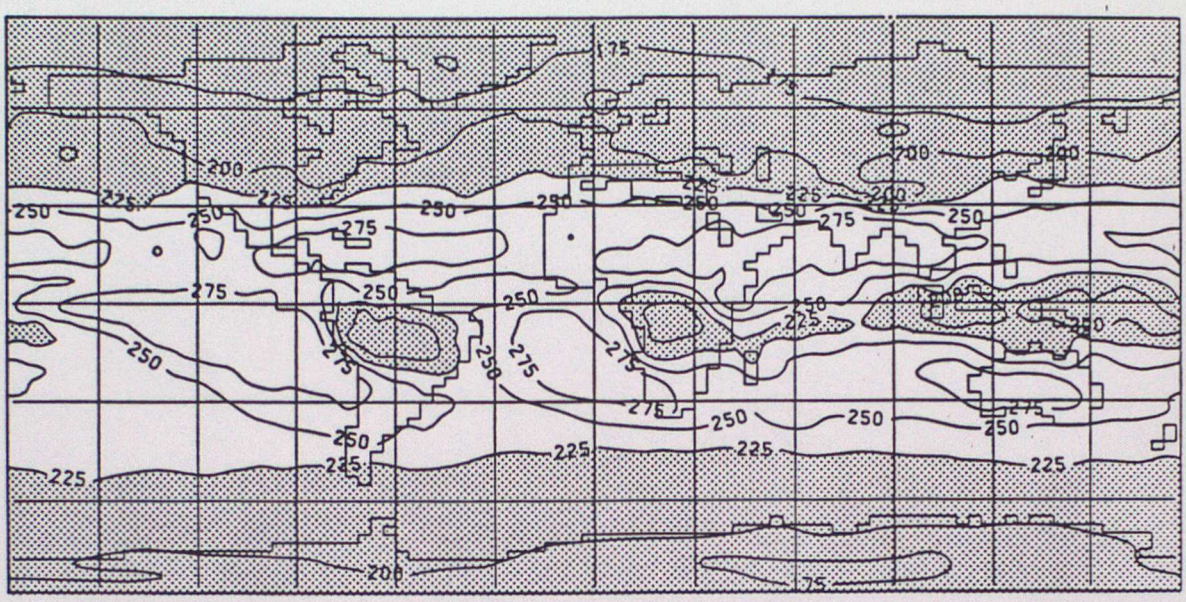

b) OLR (W m^{-2}) from new model (DJF)

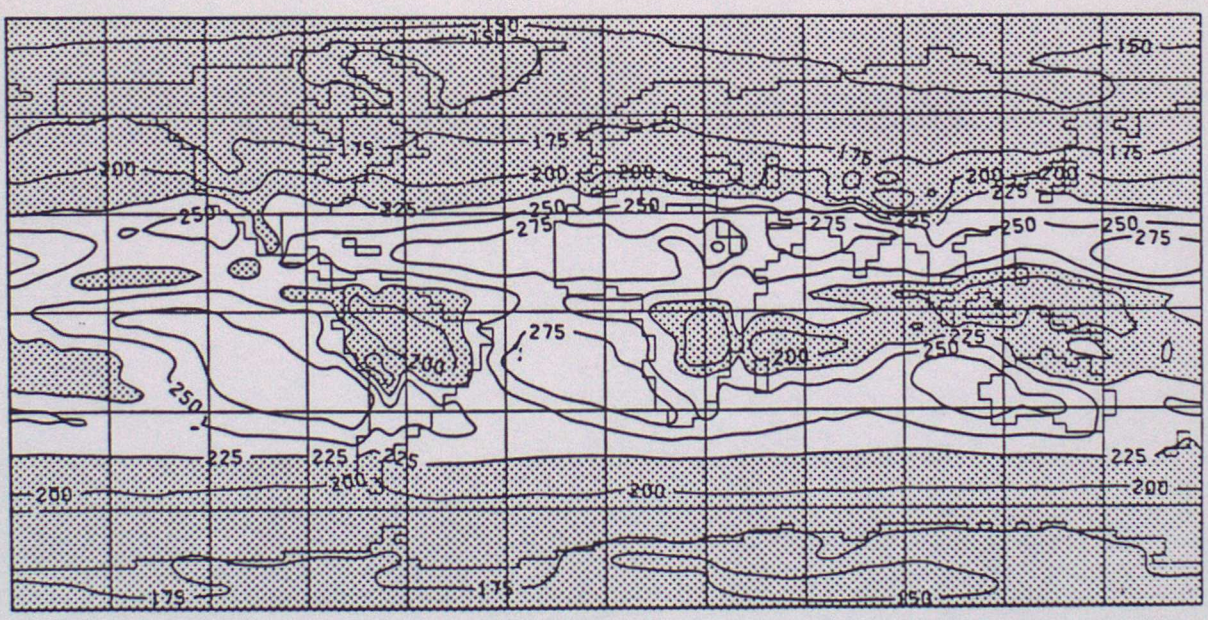

Figure 13

a) Shortwave albedo (percent) from Nimbus 7 (DJF)

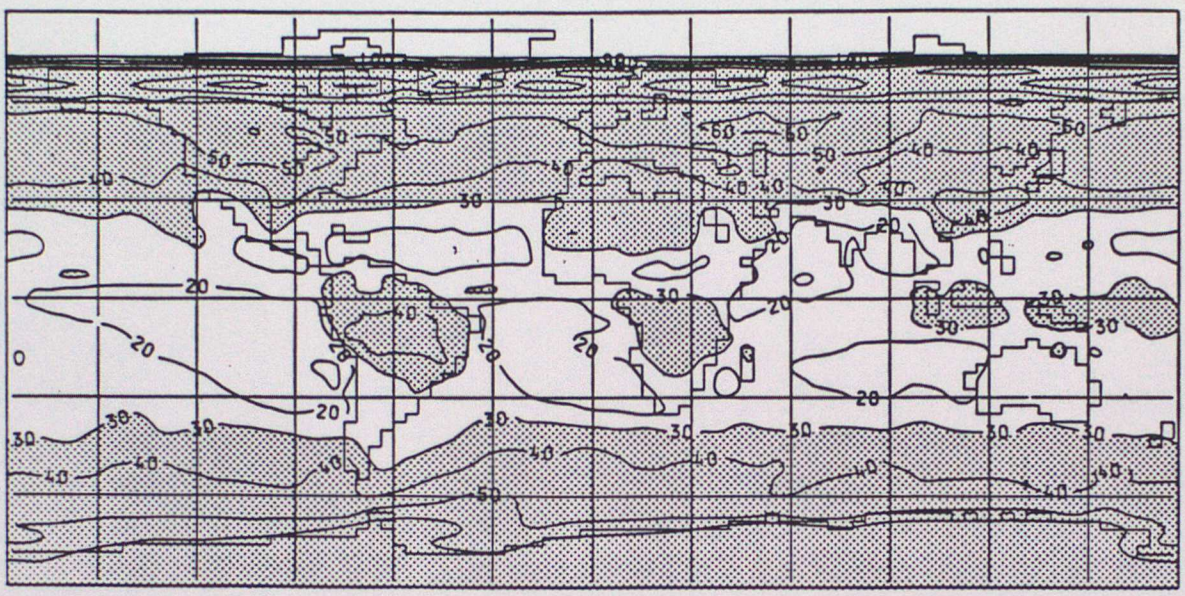

b) Shortwave albedo (percent) from new model (DJF)

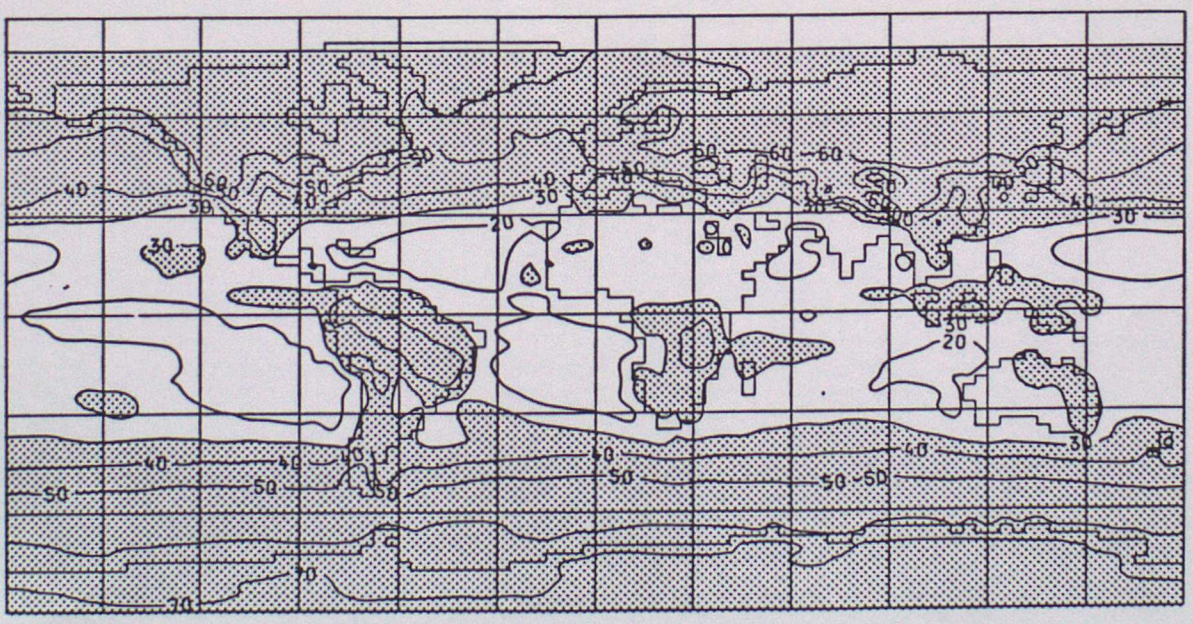

Figure 14

DYNAMICAL CLIMATOLOGY TECHNICAL NOTES

DCTN 1	June 1984	A scheme for incorporating the thermodynamic sea-ice model into a coupled ocean-atmosphere model. C Cordon and M Bottomley
DCTN 2	Sept 1984	The parametrization of the upper ocean mixed layer in coupled ocean/atmosphere models. C Cordon and M Bottomley
DCTN 3	Sept 1984	The response of a simple thermodynamic sea-ice model to GCM forcing appropriate for perennial sea-ice. M Bottomley
DCTN 4	Sept 1984	Potential vorticity in the stratosphere derived using data from satellites. S A Clough, N S Grahame and A O'Neill
DCTN 5	Sept 1984	Simulation of the seasonal cycle of SST using globally specified climatological data to force simple ocean models. N S Grahame
DCTN 6	Sept 1984	Development of an improved GCM radiation scheme. A Slingo and R C Wilderspin
DCTN 7	Sept 1984	On the specification of surface fluxes in coupled atmosphere/ocean general circulation models. J F B Mitchell, C A Wilson and C M Price
DCTN 8	Sept 1984	A survey of possible repercussions of the Soviet river reversal programme on Arctic sea-ice. H Cattle
DCTN 9	Oct 1984	A study of a strong stratospheric warming during January 1982 T D A Fairlie
DCTN 10	Nov 1984	An intercomparison of the Met O 11 M45 model and the Met O 20 11-level model on the Cyber 205 J F Dyson
DCTN 11	Nov 1984	Simulation of observed time series of temperature and precipitation over eastern England. D M Reed
DCTN 12	Nov 1984	Forecasts and analyses of the onset of the Southwest monsoon. R Kershaw
DCTN 13	Nov 1984	On modelling the effects of CO_2 on climate. J F B Mitchell
DCTN 14	Dec 1984	Development of a revised longwave radiation scheme for an atmospheric general circulation model. A Slingo and R C Wilderspin
DCTN 15	Jan 1985	Rossby wavetrains in the stratosphere forced by localised disturbances in the troposphere. C J Marks (Oxford), A O'Neill and V D Pope

DYNAMICAL CLIMATOLOGY TECHNICAL NOTES

DCTN 16	Jan 1985	Observing system experiments using the Meteorological Office's 15-level model. M A Bromley
DCTN 17	Feb 1985	Atmospheric general circulation simulation of the climate of the Mediterranean region. H Cattle
DCTN 18	Feb 1985	Diurnal variation and cloud in a general circulation model. C A Wilson and J F B Mitchell
DCTN 19	Feb 1985	The sensitivity of the Saharan region in a general circulation model. W M Cunnington and P R Rowntree
DCTN 20	Mar 1985	The impact of aircraft observations on analyses and forecasts from the operational 15-level model. B R Barwell
DCTN 21	Mar 1985	Non-linear effects on heat-induced circulation of the tropical atmosphere. A E Gill and P J Phlips
DCTN 22	Apr 1985	Simulation of cloudiness with the U.K. Meteorological Office 11-layer AGCM. A Slingo and R C Wilderspin
DCTN 23	Apr 1985	An integrated approach to the representation of cloud processes. R M B Smith
DCTN 24	May 1985	Nuclear Winter: Calculations of the shortwave radiative effects of soot aerosols. A Slingo and P Goldsmith
DCTN 25	Jul 1985	Sea ice and the Antarctic winter circulation: a numerical experiment. J F B Mitchell and T S Hills
DCTN 26	Jul 1985	A Budyko-Sellers model for study of ocean-atmosphere interaction. W J Ingram
DCTN 27	Aug 1985	The effect of a shoaling thermocline on equatorially-trapped Kelvin waves. A E Gill and B A King
DCTN 28	Sept 1985	CO_2 climate sensitivity and model dependence of results. J F B Mitchell, C A Wilson and W M Cunnington
DCTN 29	Sept 1985	Handbook of the Meteorological Office 11-layer atmospheric general circulation model. Volume 1 : Model Description Edited by A Slingo
DCTN 30	Sept 1985	Impact of land surface variations on African rainfall in general circulation models. P R Rowntree, M F Wilson and A B Sangster

DYNAMICAL CLIMATOLOGY TECHNICAL NOTES

DCTN 31 Nov 1985 The annual cycle of sea level in the eastern tropical Pacific.
C R Bigg and A E Gill

DCTN 32 Nov 1985 An analytic model of the heat-induced tropical circulation in the presence of a mean wind.
P J Phlips and A E Gill

DCTN 33 Nov 1985 The effect of resolution and diffusion on the simulated climate.
J F Dyson

DCTN 34 Jan 1986 Rossby adjustment over a step.
M K Davey, A E Gill, E R Johnson and P F Linden

DCTN 35 Jan 1986 Issues concerning the evaluation of effective surface roughness of heterogeneous terrain.
D J Carson

DCTN 36 Mar 1986 Climate sensitivity and past climates : evidence from numerical studies
J F B Mitchell

DCTN 37 Mar 1986 Parametrizations of land-surface processes in Meteorological Office numerical weather prediction and climate models
D J Carson

DCTN 38 Apr 1986 Modelling of land-surface processes and their influence on European Climate
D A Warrilow, A B Sangster and A Slingo

DCTN 39 Apr 1986 Simulation of climatic change due to increased CO_2
J F B Mitchell

DCTN 40 May 1986 On the interpretation of the Eliassen-Palm flux divergence. Part I : Theory
D G Andrews

DCTN 41 June 1986 Experiments on tropical circulation with a simple moist model.
M K Davey and A E Gill

DCTN 42 Jun 1986 Parameter regimes for studying isolated eddies.
P D Killworth and M K Davey

DCTN 43 Jun 1986 A comparison of the impact of an envelope orography and of a parametrization of orographic gravity-wave drag on model simulations.
A Slingo and D W Pearson

DCTN 44 Jul 1986 The effect of a sea-surface temperature anomaly on a prediction of the onset of the south-west monsoon over India.
R Kershaw

DCTN 45 Jul 1986 An introduction to the parametrization of land-surface processes.
D J Carson

DYNAMICAL CLIMATOLOGY TECHNICAL NOTES

DCTN 46 Sept 1986 Lateral boundaries and the heat-induced flow in the tropical atmosphere.
P J Phlips and A E Gill

DCTN 47 Nov 1986 Simulation of the diurnal cycle of outgoing longwave radiation with an atmospheric GCM.
A Slingo, R C Wilderspin and S J Brentnall

DCTN 48 Feb 1987 A 2 x CO_2 climate sensitivity experiment with a global climate model including a simple ocean
C A Wilson and J F B Mitchell

DCTN 49 Feb 1987 Sensitivity of the Met O 20 11-layer model to increased land surface roughness length
C C Heasman

DCTN 50 Feb 1987 The influence of atmospheric waves on the general circulation of the middle atmosphere
D G Andrews

DCTN 51 Feb 1987 Transport mechanisms in the middle atmosphere: an introductory survey
D G Andrews

DCTN 52 Mar 1987 The Met O 20 stratosphere-mesosphere model
M Fisher

DCTN 53 Apr 1987 Simulations of linear and nonlinear disturbances in the stratosphere
A O'Neill and V D Pope

DCTN 54 Apr 1987 Aspects of dynamics of the middle atmosphere inferred using data from a satellite and from a numerical model
T D A Fairlie and A O'Neill

DCTN 55 Apr 1987 The seasonal evolution of the stratosphere in the northern hemisphere
A O'Neill and V D Pope

DCTN 56 Apr 1987 The adjustment of numerical weather prediction models to local perturbations
B R Barwell and R A Bromley

DCTN 57 Jun 1987 Climate simulations for 9000 years before present: Seasonal variations and the effect of the Laurentide ice sheet
J F B Mitchell, N S Grahame and K J Needham

DCTN 58 Aug 1987 Climatic effects of nuclear war: the role of atmospheric stability and ground heat fluxes.
J F B Mitchell and A Slingo

DCTN 59 Oct 1987 The stratospheric major warming of winter 1984/85: observations and dynamical inferences.
T D A Fairlie and A O'Neill

DCTN 60 Oct 1987 Some comparisons between the middle atmosphere dynamics of the southern and northern hemispheres
D G Andrews

DYNAMICAL CLIMATOLOGY TECHNICAL NOTES

DCTN 61 Jan 1988 Early winter in the northern stratosphere.
M N Juckes and A O'Neill

DCTN 62 Feb 1988 Single column model tests of the Rowntree convection scheme using GATE data.
D Gregory

DCTN 63 Mar 1988 The antarctic winter; simulations with climatological and reduced sea-ice extents.
J F B Mitchell and C A Senior

DCTN 64 Mar 1988 An investigation of the Gates asynchronous coupling strategy using a simple energy-balance model.
D L Roberts